Aalborg University

Master's Thesis

A Theoretical Study of Optical Metamaterials

7th of June 2018

Authors:
Rasmus Fohlmann Andersen
Mathias Kurt Hansen

Supervisor:
Thomas Søndergaard

Preface

This thesis has been developed over the course of the 10th semester at the physics department at Aalborg University. It is worth 30 ECTS points, and is concerning the topic of Optical Metamaterials. Work on the thesis began on the 2nd of February and was handed in on the 7th of June.

Understanding the contents of this thesis and Optical Metamaterials in general, the reader should be familiar with the subject of Optics. The reader should also be experienced in Linear Algebra and Calculus.

The figures and graphs appearing throughout the report have been created in either Inkscape or Matlab unless otherwise specified. While many of the figures appearing in the report have been created in Matlab, external code [1] has been used to convert these into the *TikZ* format. Images not taken by the authors are properly cited.

As the thesis is exclusively theoretical in nature, all the work over the course of the project's creation have been in the derivation of relevant equations, and subsequently in the making of models and simulations by implementing these equations in Matlab. For this, the Matlab toolbox called 'Partial Differential Equation Toolbox' was used.

The layout of this thesis has been heavily inspired by [2].

Citations in the thesis follow the IEEE style. Thus, a citation will appear directly in the text as a number inside square brackets. The number refers to an entry in the list of references at the back of the report.

The thesis begins with an introduction in Chapter 1, which serves to familiarise the reader with the topic of Optical Metamaterials. This chapter presents the reader with the general concepts of Optical Metamaterials, and presents an

example of an Optical Metamaterial in the real world. As the *Finite Element Method* (FEM) has been used as the primary numerical method, the introduction also shortly touches upon the general concept behind this method.
Chapter 2 provides the necessary groundwork to create a foundation upon which the eventual numerical approximations are built. The length of the chapter is due to the fact that, for almost all equations used in the thesis, a derivation has been provided.
Since the development of a Matlab script has been such a large part of the thesis, the authors have chosen to include Chapter 3 to cover some of the overall steps taken in the development of the script. Excerpts of the Matlab code can be found in Appendix B.
The results gathered from the developed script are presented in Chapter 4. Many different situations are shown, among whom are scattering plots and a presentation of effective parameters of the attempted simulation of different metamaterials. This is also where a discussion of the results take place.
Finally, the thesis ends with a conclusion in Chapter 5. Here, the most significant observations are summarised. Additionally, a section covering possible future works on this topic has been provided.
Outside the main content of the thesis is an appendix. Here, a number of different interesting situations have been examined. However, the authors felt that these specific situations were not directly related to the main objective of the project, and were thus not included in the main matter of the thesis.

Lastly, we would like to thank our supervisor, Thomas Søndergaard, for the help provided throughout the development of the project.

Abstract

A Matlab script has been created to calculate the reflectance and transmittance coefficients for an array of metal cylinders, for both an s-polarised and a p-polarised incident field. The reflectance and transmittance coefficients have been used to calculate the effective parameters of the metamaterial. For the s-polarised case this went well, but the p-polarised case showed that the coefficients were dependant on the material's thickness, meaning that the material could not be approximated as a bulk material, and the effective parameters could therefore not be determined. Another Matlab script was created to calculate the scattering from an array of metal cylinders, as well as a bulk material of the same size as the array, but using the effective parameters that were determined from the reflectance and transmittance coefficients. The s-polarised case showed a reasonable agreement between the scattering calculated from the array and the scattering calculated from the bulk approximation.

Chapter 2 presents the relevant theory and derives the equations needed for the Matlab scripts. Chapter 3 describes how the structures has been created in Matlab, and how the calculations were implemented. Chapter 4 presents and discusses the results gathered with the Matlab scripts, starting with the effective parameters for variations on the metal array, and proceeds to test these with plots of the scattering of a similar array.

Contents

1 Introduction **1**

2 Theory **5**

2.1 The Wave Equations 7

2.2 The Finite Element Method 8

2.3 Calculating Reflectance and Transmittance 14

2.3.1 Non-normal incidence 23

2.3.2 S-Polarised Light 24

2.4 Scattering of Light by a Cylinder 25

2.4.1 Total Field as Basis 25

2.5 Scattered Field as Basis 29

2.5.1 Scatterer on a Surface 34

2.5.2 S-Polarised Light 35

2.6 Effective Medium Theory 35

3 Implementation **41**

3.1 Creation of Structure 43

3.2 Mesh Generation 44

3.3 Selection of Zones 46

3.4 Calculation of the Scattered Field 47

4 Results & Discussion **49**

4.1 Effective Parameters 51

4.1.1 S-Polarisation 51

4.1.2 P-Polarisation 60

4.2 Scattering 63

4.3 The Numerical Methods 70

5 Conclusion **73**

A Additional Results **81**

A.1 Effective Parameters 81

A.2 Scattering 85

A.3 Convergence 87

B Matlab Code **91**

B.1 A Matrix and M Insertion 91

B.2 Periodic Boundary Conditions 95

B.3 Calculating H' 98

B.4 Elemental Contribution to Total Field 103

List of Figures

1.1 *The Lycurgus Cup. (left) The reflection of the light on the cup causes it to appear green in colour. (right) If light is transmitted through the cup, its colour appears to be red. From [3].* 4

2.1 *An example of a unit function. It has a value of* 1 *at* $(0, 0)$ *and a value of* 0 *at* $(1, 0)$ *and* $(0, 1)$. 10

2.2 A model of the structure considered in this section. 14

2.3 A model of the structure considered in this section. 26

3.1 *An example of Constructive Solid Geometry. Face and edge labels are shown. (a) A circle overlapping a square. (b) The rectangle with the circle subtracted.* 44

3.2 *Tesselation of the CSGs found in Figure 3.1 with a* Hmax *of* 0.05. . 45

4.1 The refractive index of a square array of gold cylinders with a radius of 12 nm and a period of 30 nm. The incident field is s-polarised, i.e. the magnetic field component is parallel to the cylinders. The refractive index is calculated for an array of 10 rows thickness. . . . 51

4.2 The refractive index for bulk gold and the weighed average between the refractive index for gold and air (n=1), using for a material consisting of 50.3% gold. The refractive index of gold is calculated by linear interpolation at the given wavelength, using the data file [ref]. 52

4.3 The impedance of a square array of gold cylinders with a radius of 12 nm and a period of 30 nm. The incident field is s-polarised. The impedance is calculated for an array of 10 rows thickness. 53

4.4 The relative permittivity of a square array of gold cylinders with a radius of 12 nm and a period of 30 nm. The incident field is s-polarised. The relative permittivity is calculated for an array of 10 rows thickness. The grey dashed line marks 0 on the y-axis for easier reading. 54

4.5 The relative permeability of a square array of gold cylinders with a radius of 12 nm and a period of 30 nm. The incident field is s-polarised. The relative permeability is calculated for an array of 10 rows thickness. The grey dashed line marks 0 on the y-axis for easier reading. 55

4.6 Comparison of the real component of the refractive index of a square array of gold cylinders of varying radius. The refractive index is calculated for a array of 10 rows thickness. 56

4.7 Comparison of the imaginary component of the refractive index of a square array of gold cylinders of varying radius, with a constant period of 30 nm. The refractive index is calculated for an array of 10 rows thickness. 57

4.8 Comparison of the refractive index of a square array of either gold or silver cylinders of radius 12 nm and a period of 30 nm. The refractive index is calculated for an array of 10 rows thickness. . . . 58

4.9 Comparison of the real component of the refractive index of either a square or hexagonal array of gold cylinders of radius 12 nm and a period of 30 nm. The refractive index is calculated for an array of 10 rows thickness. 58

4.10 Comparison of the imaginary component of the refractive index of either a square or hexagonal array of gold cylinders of radius 12 nm and a period of 30 nm. The refractive index is calculated for an array of 10 rows thickness. 59

4.11 Comparison of the real part of the reflectance coefficient for a varying number of rows of a square array of gold cylinders of radius 12 nm and a period of 30 nm. 59

4.12 Comparison of the real part of the reflectance coefficient for a varying number of rows of a square array of gold cylinders of radius 12 nm and a period of 30 nm, for p-polarised light 60

4.13 Comparison of the absolute value of the reflectance coefficient for a varying number of rows of a square array of gold cylinders of radius 12 nm and a period of 30 nm, for p-polarised light 61

4.14 Comparison of the absolute of value the reflectance coefficient for a varying number of rows of a square array of gold cylinders of radius 8 nm and a period of 30 nm, for p-polarised light 62

4.15 Comparison of the imaginary part of the refractive index for a varying number of rows of a square array of gold cylinders of radius 12 nm and a period of 30 nm, for p-polarised light 63

4.16 Left: The amplitude of the total electric field for a 13 by 13 array of gold cylinders. Right: The amplitude of the total electric field for a matematerial of the same size as the 13 by 13 array, using the effective parameters presented earlier. 64

4.17 *The amplitude of the scattered electric field with the same setup as in Figure 4.16.* 64

4.18 Left: The amplitude of the scattered field for a given angle, calculated for the cylinder array. Right: The amplitude of the scattered field for a given angle, calculated with the bulk approximation. . . . 65

4.19 Left: The amplitude of the total magnetic field for a 13 by 13 array of gold cylinders. Right: The amplitude of the scattered electric field by a the same array of gold cylinders. The plots are made with an incident magnetic field which is a plane wave and parallel to the cylinders (p-polarised) and has a wavelength of 700 nm. The incident magnetic field has an amplitude of 1 and comes in from the top of the figures. The outer blue circle marks the beginning of the PML. 66

4.20 Left: The amplitude of the total electric field for a 13 by 13 array of gold cylinders, submerged halfway into a glass surface. Right: The amplitude of the total electric field for a matematerial of the same size as the 13 by 13 array, using the effective parameters. 67

4.21 The amplitude of the scattered electric field with the same setup as in Figure 4.20. 67

4.22 Left: The amplitude of the total electric field for a 13 by 13 array of gold cylinders, submerged halfway into a glass surface. Right: The amplitude of the total electric field for a matematerial of the same size as the 13 by 13 array, using the effective parameters presented earlier. The incident electric field comes in from the top left of the figures, at an angle of 45 degrees relative to the surface. 68

4.23 The amplitude of the scattered electric field with the same setup as in Figure 4.22. 68

4.24 The scattering cross section at different angles, for a 13 by 13 array of gold cylinders of radius 12 nm and period 30 nm, as well as a bulk material of same size as the array, using the corresponding effective parameters. 0 degrees corresponds to an incident field normal to the matematerial surface. The incident field is s-polarised, with an amplitude of 1. 69

4.25 The scattering cross section at different angles, for a 13 by 13 array of gold cylinders of radius 12 nm and period 30 nm, half submerged into a glass surface with refractive index 1.5, as well as a bulk material of same size as the array, using the corresponding effective parameters. 0 degrees corresponds to an incident field normal to the matematerial surface, as well as the glass surface. The incident field is s-polarised, with an amplitude of 1. 69

A.1 Left: The amplitude of the electric field throughout an array of gold cylinders with a radius of 12 nm and period of 30 nm. Right: The amplitude of the magnetic field throughout the same array. In both cases the incident field is coming in from the top and has an amplitude of 1. The circles marks the gold cylinders. 81

A.2 Comparison of the refractive index, for a array of gold cylinders with a radius of 12 nm and a period of 30 nm, and the refractive index for the same array scaled by a factor of 0.8. 82

A.3 Comparison of the real part of the impedance for a varying number of rows of a square array of gold cylinders of radius 12 nm and a period of 30 nm, for p-polarised light 82

A.4 Comparison of the imaginary part of the impedance for a varying number of rows of a square array of gold cylinders of radius 12 nm and a period of 30 nm, for p-polarised light 83

A.5 Comparison of the imaginary part of the refractive index for a varying number of rows of a square array of gold cylinders of radius 8 nm and a period of 30 nm, for p-polarised light 83

A.6 Comparison of the real part of the impedance for a varying number of rows of a square array of gold cylinders of radius 8 nm and a period of 30 nm, for p-polarised light 84

A.7 Comparison of the imaginary part of the impedance for a varying number of rows of a square array of gold cylinders of radius 8 nm and a period of 30 nm, for p-polarised light 84

A.8 Top left: The amplitude of the total electric field for a 13 by 13 array of gold cylinders. Top right: The amplitude of the total electric field for a matematerial of the same size as the 13 by 13 array, using the effective parameters presented earlier. Bottom left: The amplitude of the scattered electric field by a the same array of gold cylinders. Bottom right: The amplitude of the scattered field by the same metamaterial. All the plots are made with an incident electric field with is a plane wave and parallel to the cylinders (s-polarised) and has a wavelength of 500 nm. The incident electric field has an amplitude of 1 and comes in from the top of the figures. 85

A.9 Top left: The amplitude of the total electric field for randomly placed gold cylinders. Top right: The amplitude of the total magnetic field for randomly placed gold cylinders. Bottom left: The amplitude of the scattered electric field by randomly placed gold cylinders. Bottom right: The amplitude of the scattered magnetic field by randomly placed cylinders. All the plots are made with an incident electric or magnetic field which is a plane wave and parallel to the cylinders and has a wavelength of 700 nm, and an amplitude of 1. The metamaterial is 100 gold cylinders of radius 12, placed randomly in a circle with a radius of 100 nm. The cylinders are added till the circle is filled, with no cylinder being closer than 4 nm to another. 86

A.10 The real part of the reflectance coefficients for a square array of gold cylinders with a radius of 12 nm and a period of 30 nm, measured at different distances above the start of the first unit square, which is defined as the half a period above the centre of the first cylinder. The measurement was made with 15 rows of gold cylinders. The y-axis goes from -0.74 to -0.745. 87

A.11 The real part of the reflectance coefficients for a square array of gold cylinders with a radius of 12 nm and a period of 30 nm, calculated for meshes with different values for hmax, the largest allowed side length for a triangle. The measurement was made with 15 rows of gold cylinders. 88

A.12 The scattering cross section for an 13 by 13 array of gold cylinders, calculated with a mesh created for different values of hmax, the largest allowed side length for a triangle. The cylinders had a radius of 12 nm and a period of 30 nm. The mesh inside the cylinders were "refined" twice, meaning that each triangle were halved twice. The initial minimal triangle side length is one quarter of the hmax. . . . 88

A.13 The scattering cross section for an 390 nm by 390 nm bulk material, using the appropriate effective parameters, calculated with a mesh created for different values of hmax, the largest allowed side length for a triangle. The cylinders had a radius of 12 nm and a period of 30 nm. The mesh inside the cylinders were "refined" twice, meaning that each triangle were halved twice. The initial minimal triangle side length is one quarter of the hmax. 89

1

Introduction

As is true for many subjects in physics, the examination of metamaterial-like structures first took place at some point during the 19th century. But the term 'metamaterial' first made its appearance in the year 2000, when Smith et al. coined the term in their article concerning materials exhibiting negative-valued permittivity and permeability in the microwave spectrum [4]. These materials are also referred to as being 'left-handed', as Snell's law, for instance, would be inverted.

Conceptually, metamaterials are created by placing a number of sub-wavelength sized scatterers in a homogeneous environment, either in a periodic array or randomly. As the electromagnetic wave is unable to resolve the scatterers, it sees the collection of scatterers as an effective material with effective parameters differing from the scatterers' parameters. While numerous implementation methods exist to numerically examine metamaterials, among which are Green's Function Area Integration Method and Finite Difference Time Domain, the one used in this report is the *Finite Element Method* (FEM).
The FEM quantifies all areas by introducing a mesh of triangles of a predefined size, where a larger triangle amount yields a more accurate result, but with the added downside of a longer evaluation time. One important point to consider is the fact that the method exhibits diminishing returns with regards to accuracy versus triangle amount.
To rephrase: While the evaluation time will always have an approximately quadratic increase with an increase in triangle amount, the precision of the result will not. Thus, a balance between the two must be reached. In cases such as this, a convergence test can be a useful tool to determine at which point the model produces satisfactory results, without taking too long.

Metamaterials have the potential to be used in a lot of applications. The first known application of a metamaterial in a man-made object was the Lycurgus Cup, which was made in the 4th century. If the object is seen using light reflected on the cup's surface, it appears green in colour, while a red colour is seen if the light is transmitted through the cup. The reason for this difference in colour was found to be in how the cup was fabricated. The main material used was ruby glass, but with the essential addition of gold particles. [5]
An image of the cup in different lights can be seen in Figure 1.1.

Another rather interesting potential application of metamaterials is the creation of invisibility cloaks.

Figure 1.1: *The Lycurgus Cup. (left) The reflection of the light on the cup causes it to appear green in colour. (right) If light is transmitted through the cup, its colour appears to be red. From [3].*

2

Theory

This chapter seeks to describe the theory and show the calculations needed to derive the expressions used to obtain the results presented later in the report, as well as the theory needed to analyse these results. The starting point is Maxwell's equations, which are used to derive a wave equation for the relevant field. This wave equation is considered throughout the chapter to derive an expression of the field at a given point.

2.1 The Wave Equations

To describe the field throughout some structure, the wave equation for the given field is used. These wave equation can be derived from Maxwell's equations,

$$\nabla \cdot \vec{D} = \rho \tag{2.1}$$

$$\nabla \cdot \vec{B} = 0 \tag{2.2}$$

$$\nabla \times \vec{E} = -\frac{\partial \vec{B}}{\partial t} \tag{2.3}$$

$$\nabla \times \vec{H} = \frac{\partial \vec{D}}{\partial t} + \vec{J}, \tag{2.4}$$

where ∇ is the partial derivative in the spacial dimensions, $\vec{E}$ is the electric field, $\vec{D}$ is the electric displacement field, H is the magnetic field, $\vec{B}$ is the magnetic induction, ρ is the charge density, $\vec{J}$ is the current density and $\frac{\partial}{\partial t}$ is the partial derivative in time [6]. These can often be simplified considerably, for instance when the charge density and current density is 0, which is the case that will be considered in this section. For an incident magnetic field polarised along a z-axis, given as $H(x, y, z) = \hat{z}H(x, y)$, the wave equation can be found by considering $\nabla \times \left(\frac{1}{\epsilon}\nabla \times H\right)$, and rewriting it first using Maxwell's equations,

$$\begin{aligned} \nabla \times \left(\frac{1}{\epsilon}\nabla \times \vec{H}\right) = \nabla \times \left(\frac{1}{\epsilon}\frac{\partial \vec{D}}{\partial t}\right) \qquad & = \nabla \times \left(\frac{1}{\epsilon} i\omega\epsilon_0\epsilon\vec{E}\right) \\ = i\omega\epsilon_0 \nabla \times \vec{E} & \\ = i\omega\epsilon_0(-i\omega\mu_0\mu)\vec{H} = k^2\mu\vec{H}, & \end{aligned} \tag{2.5}$$

and then rewriting it by calculating the curl

$$\begin{aligned} \nabla \times \left(\frac{1}{\epsilon}\nabla \times \begin{bmatrix} 0 \\ 0 \\ H_z \end{bmatrix}\right) &= \nabla \times \frac{1}{\epsilon}\begin{bmatrix} \frac{\partial H_z}{\partial y} \\ \frac{\partial H_z}{\partial x} \\ 0 \end{bmatrix} \\ &= \begin{bmatrix} \frac{\partial}{\partial z}\frac{1}{\epsilon}\frac{\partial H_z}{\partial y} \\ \frac{\partial}{\partial z}\frac{1}{\epsilon}\frac{\partial H_z}{\partial x} \\ -\frac{\partial}{\partial x}\frac{1}{\epsilon}\frac{\partial H_z}{\partial x} - \frac{\partial}{\partial y}\frac{1}{\epsilon}\frac{\partial H_z}{\partial y} \end{bmatrix} \end{aligned}$$

$$
\begin{aligned}
&= \begin{bmatrix} 0 \\ 0 \\ -\frac{\partial}{\partial x}\frac{1}{\epsilon}\frac{\partial H_z}{\partial x} - \frac{\partial}{\partial y}\frac{1}{\epsilon}\frac{\partial H_z}{\partial y} \end{bmatrix} \\
&= -\frac{\partial}{\partial x}\frac{1}{\epsilon}\frac{\partial}{\partial x}\vec{H} - \frac{\partial}{\partial y}\frac{1}{\epsilon}\frac{\partial}{\partial y}\vec{H} \\
&= -\nabla \cdot \frac{1}{\epsilon}\nabla\vec{H}. \qquad (2.6)
\end{aligned}
$$

Combining Equation (2.5) and Equation (2.6) yields

$$\left(\nabla \cdot \frac{1}{\epsilon}\nabla + k^2\mu\right)\vec{H} = 0. \qquad (2.7)$$

Using the same approach for the electric field yields

$$\left(\nabla \cdot \frac{1}{\mu}\nabla + k^2\epsilon\right)\vec{E} = 0. \qquad (2.8)$$

2.2 The Finite Element Method

This section is largely based on [7].

In general terms, the FEM is a numerical method used to approximate a solutions for boundary value problems. The method simplifies a problem by tessellating the desired geometry intro smaller geometrical shapes such as triangles or quadrilaterals. The simplification of the problem lies in the act of treating every element as a problem of its own, and since every element of the created mesh contains a number of vertices (called nodes), which are often shared by multiple elements, one simply has to find a way to relate each elements with one another. Usually one begins with a partial differential equation which describes the situation perfectly. As these differential equations can have an infinite amount of solutions, and since usually a specific, unique solution is desired, one must specify a set of *Dirichlet* (also known as first-type) boundary conditions. The way in which the solution is found, is by coming up with a series of linear equation for each of the nodes. Giving each node a unique number, one can insert these linear equations into a matrix and find the complete solution.

The actual equations are found using the *Galerkin* approach, which is a weighted-residual method. The differential equations dealt with in this report are of second order. These are originally given in their strong form, and, along with their accompanying boundary conditions, they must be converted into an *integro-differential* formulation. The general idea is to multiply both sides of the differential equations with a weight function, and then taking an integral over the domain of the element in question. By using integration by parts, one will find that the function appearing in a second order differential equation, which would otherwise have to be twice differentiable, need only be once differentiable. The second differentiation has been assigned to the weight function. Since the restriction on the shape function has been lessened, this approach is also known as the *weak formulation*. For the method to be called the *Galerkin method*, the weight-functions used must be from the same set as the shape functions.

In this report, it is sought to calculate the magnetic field throughout a predefined structure. Triangles are chosen as the shapes used in the tessellation of the geometry. Thus, each element has three nodes, unless, for instance, a quadratic shape function is used. In that case, it is necessary to introduce additional nodes in the middle of each elemental segment. In this report, however, linear shape functions have been used.
The size of the elements in the mesh need not be the same. This is useful in cases where specific, rapidly numerically varying areas are known. In such areas, one can force the mesh to have a higher resolution. Since the method finds values for the nodes in the mesh and not the elements themselves, it is necessary to fashion a way to find the values within the area of the elements. This can be done by assuming that the field at any point inside an element is a linear combination of the fields at each vertex, with the closest vertex contributing the most to the field. One way of achieving this is by introducing a unit triangle in a (u, v) coordinate system, described by the points $(0, 0)$, $(0, 1)$ and $(1, 0)$. These 3 unit equations have the values of 1 at one of the vertices, which then decrease to 0 as the opposite

vertices are reached. These equations can be found in Equation (2.9).

$$\begin{aligned} f_1(u,v) &= 1-u-v, \\ f_2(u,v) &= u, \\ f_3(u,v) &= v. \end{aligned} \tag{2.9}$$

The first of these functions can be seen in Figure 2.1.

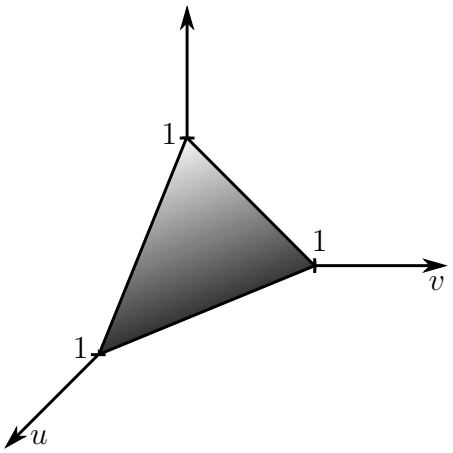

Figure 2.1: *An example of a unit function. It has a value of* 1 *at* $(0,0)$ *and a value of* 0 *at* $(1,0)$ *and* $(0,1)$.

Resonance in Nano Particles

We will examine the frequencies of the electric field which results in resonance in particles that are much smaller than the wavelength of the light in some or all directions. Generally, we can express the electric field as the gradient of some scalar field:

$$\vec{E}_i = -\nabla\phi_i \quad i = 1,2, \tag{2.10}$$

where $\vec{E}_1$ is the field outside the particle, and $\vec{E}_2$ is the field inside the particle. Assuming there is no free charges, Gauss's Law gives

$$\nabla \cdot \vec{E} = 0 \tag{2.11}$$

$$\nabla^2 \phi = 0. \tag{2.12}$$

This gives a differential equation which has to be solved. Requiring that the component of the electric field which is tangential to the surface and the component of the displacement field which is normal to the surface is continuous at the surface (no surface charge) gives the following boundary conditions [6],

$$\phi_1(\vec{p}) = \phi_2(\vec{p}) \quad p \in \Omega \tag{2.13}$$

$$\epsilon_1 \frac{d\phi_1(\vec{p})}{d\vec{p}}\bigg|_{p=q} = \epsilon_2 \frac{d\phi_2(\vec{p})}{d\vec{p}}\bigg|_{p=q} \quad q \in \Omega \tag{2.14}$$

where Ω is the surface of the particle. In this case the particle will be a cylindrical particle, with its ground area in the x, y-plane, and the height along the z-axis. Additionally, the direction of the electric field will be along the z-axis, $\vec{E}(\vec{p}) = E_0(x, y)\hat{z}$. To determine the field inside and outside the particle, we need a guess for the two scalar fields:

$$\phi_1(r, \theta) = -E_0 r \cos\theta + A\frac{\cos\theta}{r} \tag{2.15}$$

$$\phi_2(r, \theta) = Br\cos\theta \tag{2.16}$$

We need to verify that these fulfill the differential equation, described by Equation (2.12). In polar coordinates, the Laplace operator is given by [8]

$$\nabla^2 = \frac{1}{r}\frac{\partial}{\partial r}\left(r\frac{\partial f}{\partial r}\right) + \frac{1}{r^2}\frac{\partial^2 f}{\partial \theta^2}. \tag{2.17}$$

Using this to test the guesses for the fields gives,

$$\begin{aligned} r\frac{\partial\phi_1(r,\theta)}{\partial r} = a &= -E_0 r\cos\theta - A\frac{\cos\theta}{r} \\ \frac{1}{r}\frac{\partial a}{\partial r} &= \frac{-E_0\cos\theta}{r} + A\frac{\cos\theta}{r^3} \\ \frac{1}{r^2}\frac{\partial^2\phi_1(r,\theta)}{\partial\theta^2} &= \frac{E_0\cos\theta}{r} - A\frac{\cos\theta}{r^3} \end{aligned} \tag{2.18}$$

From this it can be seen that ϕ_1 satisfies Equation (2.12). The same is true for ϕ_2:

$$\begin{aligned} \frac{1}{r}\frac{\partial}{\partial r}\left(r\frac{\partial\phi_2(r,\theta)}{\partial r}\right) &= \frac{B}{r}\cos\theta \\ \frac{1}{r^2}\frac{\partial^2\phi_2(r,\theta)}{\partial\theta^2} &= -\frac{B}{r}\cos\theta \end{aligned} \tag{2.19}$$

Using the conditions described by Equation (2.13) and Equation (2.14) the values of A and B can be determined. Using Equation (2.13) to get an expression for B gives

$$\begin{aligned} \phi_1(a,\theta) &= \phi_2(a,\theta) \\ -E_0 a\cos(\theta) + \frac{A}{a}\cos\theta &= Ba\cos\theta \\ B &= -E_0 + \frac{A}{a^2}. \end{aligned} \tag{2.20}$$

Using Equation (2.14) to get another expression for B gives

$$\begin{aligned} \epsilon_1\frac{\partial\phi_1(r,\theta)}{\partial r}\bigg|_{r=a} &= \epsilon_2\frac{\partial\phi_2(r,\theta)}{\partial r}\bigg|_{r=a} \\ \epsilon_1\left(-E_0\cos\theta - A\cos\theta\frac{1}{a^2}\right) &= \epsilon_2 B\cos\theta \\ B &= -\frac{\epsilon_1}{\epsilon_2}\left(\frac{A}{a^2} + E_0\right). \end{aligned} \tag{2.21}$$

The equations Equation (2.20) and Equation (2.21) can be combined to get an expression for A,

$$\begin{aligned} -\frac{\epsilon_1}{\epsilon_2}\left(\frac{A}{a^2}+E_0\right) &= \frac{A}{a^2}-E_0 \\ \frac{A}{a^2}\left(1+\frac{\epsilon_1}{\epsilon_2}\right) &= E_0\left(1-\frac{\epsilon_1}{\epsilon_2}\right) \\ A &= E_0 a^2 \frac{\epsilon_2-\epsilon_1}{\epsilon_2+\epsilon_1}. \end{aligned} \tag{2.22}$$

With A calculated, B can now be calculated,

$$B = E_0\left(\frac{\epsilon_2-\epsilon_1}{\epsilon_2+\epsilon_1}-1\right) = E_0\frac{2\epsilon_2}{\epsilon_2+\epsilon_1}. \tag{2.23}$$

By inserting the expressions for A and B, the field inside and outside the particle can be expressed in terms of the incident field. The field outside the particle is given as

$$\phi_1(r,\theta) = -E_0 r\cos\theta + E_0\frac{a^2}{r}\frac{\epsilon_2-\epsilon_1}{\epsilon_2+\epsilon_1}\cos\theta = E_0\cos\theta\left(\frac{a^2}{r}\frac{\epsilon_2-\epsilon_1}{\epsilon_2+\epsilon_1}-r\right) \tag{2.24}$$

$$E_1(r,\theta) = \nabla\phi_1(r,\theta) = E_0\cos\theta\left(-\frac{a^2}{r^2}\frac{\epsilon_2-\epsilon_1}{\epsilon_2+\epsilon_1}-1\right)\hat{r} - E_0\sin\theta\left(\frac{a^2}{r^2}\frac{\epsilon_2-\epsilon_1}{\epsilon_2+\epsilon_1}-1\right)\hat{\theta}. \tag{2.25}$$

The field inside the particle is given as

$$\phi_2(r,\theta) = r\cos\theta E_0\frac{2\epsilon_2}{\epsilon_2+\epsilon_1} \tag{2.26}$$

$$E_2(r,\theta) = \nabla\phi_2(r,\theta) = \cos\theta E_0\frac{2\epsilon_2}{\epsilon_2+\epsilon_1}\hat{r} - \sin\theta E_0\frac{2\epsilon_2}{\epsilon_2+\epsilon_1}\hat{\theta} \tag{2.27}$$

As ϵ_2 is a function of the wavelength, there might be certain wavelengths where $\epsilon_2 \approx \epsilon_1$, which results in a small denominator in Equation (2.27), and thereby a strong field inside the particle.

2.3 Calculating Reflectance and Transmittance

In order to calculate the reflectance and transmittance coefficients for a slab of metamaterial, the field has to be calculated throughout the structure. For this section the structure is a periodic array of metal cylinders, and the field is parallel to the cylinders. Because of these restrictions, the structure can be seen as being two-dimensional and to only be a single period wide. The structure is illustrated in Figure 2.2. The finite element method is used, which means that the structure

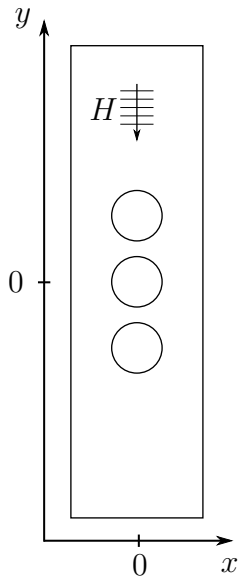

Figure 2.2: A model of the structure considered in this section.

will be divided into triangles, and the field inside a triangle will be approximated as

$$H(u,v) = \sum_{i=1}^{3} a_i f_i(u,v), \tag{2.28}$$

where a_i is the field at a certain vertex, and f_i is the corresponding unit function. The following calculations are made with the help from [9]. To describe the field throughout the structure, the wave equation for the field is considered,

$$\left(\nabla \frac{1}{\epsilon} \nabla + k_0^2\right) H(x,y) = 0. \tag{2.29}$$

Using the Galerkin approach [7] leads to the following integral,

$$\int w(x,y)\left(\nabla\frac{1}{\epsilon}\nabla + k_0^2\right)H(x,y)dydx = 0 \tag{2.30}$$

Using the product rule for differentiation, this can be rewritten;

$$\begin{aligned}\nabla\cdot\left(w(x,y)\frac{1}{\epsilon}\nabla H(x,y)\right) &= \nabla w(x,y)\cdot\left(\frac{1}{\epsilon}\nabla H(x,y)\right) + w(x,y)\nabla\cdot\left(\frac{1}{\epsilon}\nabla H(x,y)\right)\\ w(x,y)\nabla\cdot\left(\frac{1}{\epsilon}\nabla H(x,y)\right) &= \nabla\cdot\left(w(x,y)\frac{1}{\epsilon}\nabla H(x,y)\right) - \nabla w(x,y)\cdot\left(\frac{1}{\epsilon}\nabla H(x,y)\right)\end{aligned} \tag{2.31}$$

Inserting this in Equation (2.30) gives

$$\begin{aligned}\int_A w(x,y)\left(\nabla\frac{1}{\epsilon}\nabla + k_0\right)H(x,y)dydx = &\int_A \nabla\cdot\left(w(x,y)\frac{1}{\epsilon}\nabla H(x,y)\right)dydx\\ &-\int_A \nabla w(x,y)\cdot\left(\frac{1}{\epsilon}\nabla H(x,y)\right)dydx\\ &+\int_A w(x,y)k_0^2H(x,y)dydx\\ &=0\end{aligned} \tag{2.32}$$

The first integral on the right-hand side of Equation (2.32) can be rewritten as a curve integral using Gauss' divergence theorem [8],

$$\int_A \nabla\cdot\vec{V}(\vec{r})dA = \int_{dA}\hat{n}\cdot\vec{V}(\vec{r})dl \tag{2.33}$$

$$\int_A \nabla\cdot\left(w(x,y)\frac{1}{\epsilon}\nabla H(x,y)\right)dydx = \oint_l \hat{n}\cdot\left(w(x,y)\frac{1}{\epsilon}\nabla H(x,y)\right)dl \tag{2.34}$$

When evaluating the curve integral around a triangle element, each contribution will be cancelled out by the contributions from the neighbouring triangles, as the only thing that is different along the same line in the neighbouring triangle is the sign of the normal vector. This means that the curve integral will only give any contributions along the edges of the structure. Due to the periodic boundary

conditions along the left and right edges, these contributions will also cancel out leaving only the contributions from the top and the bottom. For an incident field running along the y-axis in the negative direction, and with unit amplitude, the incident field is given as $H_0(x,y) = e^{-ik_o n_1 y}$, and the field at a sufficiently large distance from the metal cylinders is given by $H(x,y) \approx H_0 + Ae^{\pm ik_0 n_1 y}$, where $+$ is taken for the field above the cylinders, and $-$ is taken below. Inserting this expression for $H(x,y)$ in the the curve integral gives

$$\begin{aligned}\oint_l \hat{n} \cdot \left(w(x,y)\frac{1}{\epsilon}\nabla H(x,y) \right) dl &= \oint_l \hat{n} \cdot w(x,y)\frac{1}{\epsilon}\hat{y}\left(-ik_0 n_1 H_0 \pm ik_0 n_1 A e^{\pm ik_o n_1 y}\right) dl \\ &= \oint_l \mp ik_0 n_1 (x,y)\frac{1}{\epsilon}H_0(x,y) + ik_0 n_1 w \frac{1}{\epsilon}(H(x,y) - H_0(x,y))dl \\ &= \oint_l -ik_0 n_1 w(x,y)\frac{1}{\epsilon}H_0(x,y)(1 \pm 1)dl + \oint_l ik_0 n_1 w(x,y)\frac{1}{\epsilon}H(x,y)dl\end{aligned} \tag{2.35}$$

Inserting Equation (2.35) in Equation (2.32) gives

$$\begin{aligned}&-\int_A \nabla w(x,y) \cdot \left(\frac{1}{\epsilon}\nabla H(x,y)\right) dydx + \int_A w(x,y)k_0^2 H(x,y)dydx \\ &+ \oint_l ik_0 n_1 w(x,y)\frac{1}{\epsilon}H(x,y)dl - \oint_l ik_0 n_1 w(x,y)\frac{1}{\epsilon}H_0(x,y)(1 \pm 1)dl = 0\end{aligned} \tag{2.36}$$

With the field expressed as in Equation (2.28), and using the unit functions from Equation (2.9) as the weight functions, the first three integrals of the left-hand side of Equation (2.36) will be of $\sum_{j=1}^{3} f_j \sum_{i=1}^{3} f_i a_i$, or a derivative thereof, while the last integral is of the form $\sum_{i=1}^{3} f_i a_i$. Moving the last term to the right-hand side, this can be expressed as an equation of 3×3 matrices

$$\left(-\mathbf{A}^{(k)} + \mathbf{B}^{(k)} + \mathbf{C}^{(k)}\right) \begin{bmatrix} a_1^{(k)} \\ a_2^{(k)} \\ a_3^{(k)} \end{bmatrix} = \begin{bmatrix} b_1^{(k)} \\ b_2^{(k)} \\ b_3^{(k)} \end{bmatrix} \tag{2.37}$$

where

$$A_{i,j}^{(k)} = \frac{1}{\epsilon}\int \nabla f_i(u,v)\cdot\nabla f_j(u,v)dxdy, \tag{2.38}$$

$$B_{i,j}^{(k)} = k_0^2\int f_i(u,v)f_j(u,v)dxdy \tag{2.39}$$

$$C_{i,j}^{(k)} = \frac{ik_0n_1}{\epsilon}\oint f_i(u,v)f_j(u,v)dl \tag{2.40}$$

$$b_i^{(k)} = ik_0n_1H_0(1\pm 1)\oint f_i(u,v)dl \tag{2.41}$$

Now these four elements has to be calculated, starting with **A**. As the unit functions f are defined on some (u,v)-coordinate system, ∇ has to be expressed as $\nabla = \hat{x}\left(\frac{\partial f}{\partial u}\frac{\partial u}{\partial x}+\frac{\partial f}{\partial v}\frac{\partial v}{\partial x}\right)+\hat{y}\left(\frac{\partial f}{\partial u}\frac{\partial u}{\partial y}+\frac{\partial f}{\partial v}\frac{\partial v}{\partial y}\right)$. Starting with $A_{1,1}$, we look at $f_1(u,v) = 1-u-v$, and the gradient is given by

$$\nabla f_1(u,v) = \hat{x}\left(-1\frac{\partial u}{\partial x}-1\frac{\partial v}{\partial x}\right)+\hat{y}\left(-1\frac{\partial u}{\partial y}-1\frac{\partial v}{\partial y}\right) \tag{2.42}$$

$$\nabla f_1(u,v)\cdot\nabla f_1(u,v) = \left(\frac{\partial u}{\partial x}+\frac{\partial v}{\partial x}\right)^2+\left(\frac{\partial u}{\partial y}+\frac{\partial v}{\partial y}\right)^2 \tag{2.43}$$

To calculate the derivatives of u and v with respect to x and y, we consider how they are defined. As u and v maps the vertices of a triangle onto the vertices of a unit triangle, we can write

$$\vec{r} = \vec{r}_1+u(\vec{r}_2-\vec{r}_1)+v(\vec{r}_3-\vec{r}_1) \tag{2.44}$$

$$\vec{r}-\vec{r}_1 = u(\vec{r}_2-\vec{r}_1)+v(\vec{r}_3-\vec{r}_1) \tag{2.45}$$

$$x-x_1 = u(x_2-x_1)+v(x_3-x_1) \tag{2.46}$$

$$y-y_1 = u(y_2-y_1)+v(y_3-y_1) \tag{2.47}$$

where $\vec{r}$ is a point inside a triangle, and $\vec{r}_n$ marks the n'th vertex. From this u and v can be isolated. Multiplying Equation (2.46) by (y_3-y_1) and Equation (2.47)

by $(x_3 - x_1)$, and subtracting one from the other gives

$$(x - x_1)(y_3 - y_1) = u(x_2 - x_1)(y_3 - y_1) + v(x_3 - x_1)(y_3 - y_1) \tag{2.48}$$

$$(y - y_1)(x_3 - x_1) = u(y_2 - y_1)(x_3 - x_1) + v(y_3 - y_1)(x_3 - x_1) \tag{2.49}$$

$$(x - x_1)(y_3 - y_1) - (y - y_1)(x_3 - x_1) = u(x_2 - x_1)(y_3 - y_1) - u(y_2 - y_1)(x_3 - x_1) \tag{2.50}$$

$$u = \frac{(x - x_1)(y_3 - y_1) - (y - y_1)(x_3 - x_1)}{(x_2 - x_1)(y_3 - y_1) - (y_2 - y_1)(x_3 - x_1)} \tag{2.51}$$

$$v = \frac{(x - x_1)(y_2 - y_1) - (y - y_1)(x_2 - x_1)}{(x_3 - x_1)(y_2 - y_1) - (y_3 - y_1)(x_2 - x_1)}, \tag{2.52}$$

where v was obtained by instead multiplying by $(y_2 - y_1)$ and $(x_2 - x_1)$. From this we can obtain the derivatives:

$$\frac{\partial u}{\partial x} = \frac{y_3 - y_1}{(x_2 - x_1)(y_3 - y_1) - (y_2 - y_1)(x_3 - x_1)} \tag{2.53}$$

$$\frac{\partial u}{\partial y} = \frac{-(x_3 - x_1)}{(x_2 - x_1)(y_3 - y_1) - (y_2 - y_1)(x_3 - x_1)} \tag{2.54}$$

$$\frac{\partial v}{\partial x} = \frac{y_2 - y_1}{(x_3 - x_1)(y_2 - y_1) - (y_3 - y_1)(x_2 - x_1)} \tag{2.55}$$

$$\frac{\partial v}{\partial y} = \frac{-(x_2 - x_1)}{(x_3 - x_1)(y_2 - y_1) - (y_3 - y_1)(x_2 - x_1)} \tag{2.56}$$

With this, $A_{1,1}^{(k)}$ can be expressed as

$$\begin{aligned} A_{1,1}^{(k)} &= \frac{1}{\epsilon^{(k)}} \int \left(\frac{\partial u}{\partial x} + \frac{\partial v}{\partial x}\right)^2 + \left(\frac{\partial u}{\partial y} + \frac{\partial v}{\partial y}\right)^2 dxdy \\ &= \frac{1}{\epsilon^{(k)}} \left(\left(\frac{\partial u}{\partial x} + \frac{\partial v}{\partial x}\right)^2 + \left(\frac{\partial u}{\partial y} + \frac{\partial v}{\partial y}\right)^2\right) \int 1 dxdy \\ &= \frac{A^{(k)}}{\epsilon^{(k)}} \left(\left(\frac{\partial u}{\partial x} + \frac{\partial v}{\partial x}\right)^2 + \left(\frac{\partial u}{\partial y} + \frac{\partial v}{\partial y}\right)^2\right) \end{aligned} \tag{2.57}$$

The remaining entries of $\mathbf{A}^{(k)}$ can be calculated in a similar way. The full matrix is given by

$$\mathbf{A}^{(k)} = \frac{A^{(k)}}{\epsilon^{(k)}} \begin{bmatrix} \left(\frac{\partial u}{\partial x} + \frac{\partial v}{\partial x}\right)^2 + \left(\frac{\partial u}{\partial y} + \frac{\partial v}{\partial y}\right)^2 & -\left(\frac{\partial u}{\partial x} + \frac{\partial v}{\partial x}\right)\frac{\partial u}{\partial x} - \left(\frac{\partial u}{\partial y} - \frac{\partial v}{\partial y}\right)\frac{\partial u}{\partial y} & -\left(\frac{\partial u}{\partial x} + \frac{\partial v}{\partial x}\right)\frac{\partial v}{\partial x} - \left(\frac{\partial u}{\partial y} - \frac{\partial v}{\partial y}\right)\frac{\partial v}{\partial y} \\ -\left(\frac{\partial u}{\partial x} + \frac{\partial v}{\partial x}\right)\frac{\partial u}{\partial x} - \left(\frac{\partial u}{\partial y} - \frac{\partial v}{\partial y}\right)\frac{\partial u}{\partial y} & \left(\frac{\partial u}{\partial x}\right)^2 + \left(\frac{\partial u}{\partial y}\right)^2 & \frac{\partial v}{\partial x}\frac{\partial u}{\partial x} + \frac{\partial v}{\partial y}\frac{\partial u}{\partial y} \\ -\left(\frac{\partial u}{\partial x} + \frac{\partial v}{\partial x}\right)\frac{\partial v}{\partial x} - \left(\frac{\partial u}{\partial y} - \frac{\partial v}{\partial y}\right)\frac{\partial v}{\partial y} & \frac{\partial v}{\partial x}\frac{\partial u}{\partial x} + \frac{\partial v}{\partial y}\frac{\partial u}{\partial y} & \left(\frac{\partial v}{\partial x}\right)^2 + \left(\frac{\partial v}{\partial y}\right)^2 \end{bmatrix} \tag{2.58}$$

Note that the values of the derivatives depends on the coordinates for the vertices of the triangle. Next is the $\mathbf{B}$ matrix. Looking at the $B_{2,2}$ entry, it is given by

$$B_{2,2}^{(k)} = k_0^2 \int u^2 dxdy \tag{2.59}$$

The integral can be changed from an integral over x and y to an integral over u and v using

$$\begin{aligned} dxdy &= \left|\frac{\partial x}{\partial u}\frac{\partial y}{\partial v} - \frac{\partial y}{\partial u}\frac{\partial x}{\partial v}\right| dudv \\ &= \frac{A^{(k)}}{A_{unit}} dudv \\ &= 2A^{(k)} dudv, \end{aligned} \tag{2.60}$$

where A_{unit} is the area of the unit triangle, which is $\frac{1}{2}$. Inserting this in Equation (2.59) gives

$$\begin{aligned} B_{2,2}^{(k)} &= 2k_0^2 A^{(k)} \int_0^1 \int_0^{1-v} u^2 dudv \\ &= \frac{2}{3} k_0^2 A^{(k)} \int_0^1 (1-v)^3 dv \\ &= \frac{2}{12} k_0^2 A^{(k)} \end{aligned} \tag{2.61}$$

The full $\mathbf{B}$ matrix is given by

$$\mathbf{B}^{(k)} = \frac{k_0^2 A^{(k)}}{12} \begin{bmatrix} 2 & 1 & 1 \\ 1 & 2 & 1 \\ 1 & 1 & 2 \end{bmatrix} \tag{2.62}$$

The $\mathbf{C}$ matrix is a line integral over the upper or lower edge of the main structure. As the unit functions are defined so that they are equal to 1 at one vertex, and 0 at the opposing edge, one of the unit functions will be 0 along the edge where the line integral is carried out. This means that all the integrals involving this unit function is equal to 0, so only four of the nine entries in the matrix are different from 0. Assuming that vertex one and two are the ones that are on the edge, the entry $C_{1,1}$ can be calculated as

$$\begin{aligned} C_{2,2}^{(k)} =& \frac{ik_0 n_1}{\epsilon^{(k)}} \oint u^2 dl \\ =& l^{(k)} \frac{ik_0 n_1}{\epsilon^{(k)}} \oint_0^1 u^2 du \\ =& l^{(k)} \frac{ik_0 n_1}{\epsilon^{(k)}} \frac{1}{3}, \end{aligned} \tag{2.63}$$

where l is the length of the edge. The full $\mathbf{C}$ matrix is then given as

$$\mathbf{C}^{(k)} = \frac{l^{(k)}}{6} \frac{ik_0 n_1}{\epsilon^{(k)}} \begin{bmatrix} 2 & 1 & 0 \\ 1 & 2 & 0 \\ 0 & 0 & 0 \end{bmatrix} \tag{2.64}$$

The $\vec{b}^{(k)}$ vector is the only part left to calculate. The (1 ± 1) part depends on whether an edge of the triangle is on the upper or lower edge of the structure, with + corresponding to the upper edge. This means that the only contributions will come from the line integrals along the upper edge. Similarly to the $\mathbf{C}^{(k)}$ matrix, one of the unit functions will be 0 along the edge, meaning only two of the entries will be different from 0. As the integral is simply a line integral over a function which goes linearly from 0 to 1 (or 1 to 0), the value of the integral is half the length of the line. If the two point that are placed on the edge are the

first two points, the $\vec{b}$ vector is given by

$$\vec{b}^{(k)} = \frac{l^{(k)}}{2} i k_0 n_1 H_0 \begin{bmatrix} 1 \\ 1 \\ 0 \end{bmatrix} \tag{2.65}$$

With these four elements, the equations for a single triangle element is described, and the next step is to combine the equations for each triangle element, to describe the field throughout the entire structure. The $\vec{a}$ vector is related to the field as

$$\begin{bmatrix} a_1^{(k)} \\ a_2^{(k)} \\ a_3^{(k)} \end{bmatrix} = \mathbf{P}^{(k)} \begin{bmatrix} H_1 \\ H_2 \\ \vdots \\ H_N \end{bmatrix}. \tag{2.66}$$

Adding the equations from each triangle gives

$$\sum_{k=1}^{N} \mathbf{P}^{(k),T} \left(-\mathbf{A}^{(k)} + \mathbf{B}^{(k)} + \mathbf{C}^{(k)} \right) \mathbf{P}^{(k)} \begin{bmatrix} H_1 \\ H_2 \\ \vdots \\ H_N \end{bmatrix} = \sum_{k=1}^{N} \begin{bmatrix} b_1^{(k)} \\ b_2^{(k)} \\ b_3^{(k)} \end{bmatrix}$$

$$\mathbf{M} \begin{bmatrix} H_1 \\ H_2 \\ \vdots \\ H_N \end{bmatrix} = \begin{bmatrix} b_1 \\ b_2 \\ \vdots \\ b_N \end{bmatrix} \tag{2.67}$$

$$\begin{bmatrix} H_1 \\ H_2 \\ \vdots \\ H_N \end{bmatrix} = \mathbf{M}^{-1} \vec{b}_v \tag{2.68}$$

When this equation is solved, the field is known at every vertex of the triangles throughout the structure. However, before this equation can be solved, some boundary conditions has to be imposed. As the goal is to model the field throughout a periodic array of cylinders, the structure is also considered to be periodic along the x-axis. This means that for a given point on the left edge of the structure, the field should be the same at the same for the same y-coordinate on the

right edge of the structure.

This boundary condition requires that the vertices along one edge is closely matched in height to the vertices along the other edge. Once two edge vertices with the same heigth has been found, $\mathbf{M}$ and $\vec{b}_v$ has to be modified. Assuming that the points numbered n and m are the ones that are paired up, the n'th row of the $\mathbf{M}$ matrix should be set to 0, while the n'th and m'th entries in this row should be set to 1 and -1 respectively. In the $\vec{b}_v$ vector, the n'th and m'th entry should be set to zero:

$$\mathbf{M} = \begin{bmatrix} & & & & & \vdots & & & & \\ 0 & \dots & 0 & M_{n,n} = 1 & 0 & \dots & 0 & M_{n,m} = -1 & 0 & \dots \\ & & & & & \vdots & & & & \end{bmatrix}, \ \vec{b}_v = \begin{bmatrix} b_1 \\ \vdots \\ b_n = 0 \\ \vdots \\ b_m = 0 \\ \vdots \end{bmatrix} \tag{2.69}$$

Inserting these corrections in Equation (2.67) will lead to the equation

$$H_n - H_m = 0, \tag{2.70}$$

which fulfills the boundary condition for those points. Doing this for all the points along the edges fulfills the boundary condition for the entire structure.

With this boundary condition imposed, Equation (2.68) can be calculated. With the field calculated, the reflectance and transmittance coefficients can be calculated, by considering the field at a point above and below the cylinder region. The field should be taken at points that are sufficiently far away from the cylinders, so that any evanescent waves are gone, and the reflected and transmitted waves can be considered plane waves. Under these conditions, the reflectance coefficient

can be found as

$$H(x,y) = H_0(x,y) + H_r(x,y) \quad y > y_0$$
$$H(x,y) = e^{-ik_0 n_1 y} + e^{-ik_0 n_1 y_0} r e^{ik_0 n_1 (y-y_0)} \tag{2.71}$$
$$r = \left(H(x,y) - H_0(x,y)\right) e^{2ik_0 n_1 y_0} e^{-ik_0 n_1 y}, \tag{2.72}$$

and the transmittance coefficient can be found as

$$H(x,y) = e^{-ik_0 n_1 (y_0)} t H_0(x,y) \quad y < -y_0 \tag{2.73}$$
$$t = H(x,y) e^{ik_0 n_1 y_0} e^{ik_0 n_1 (y+y_0)} \tag{2.74}$$

2.3.1 Non-normal incidence

So far all the calculations has been done under the assumption that the light hits the metamaterial at normal incidence. However, as metamaterials can often be anisotropic, the effective refractive index might change depending on the angle of incidence. Taking into account that the angle of incidence can be different from normal incidence changes some of the equations, but only slightly. The calculations for normal incidence used an incident field given as

$$H_0(x,y) = e^{-ik_0 n_1 y}, \tag{2.75}$$

whereas an incident field with an angle θ (relative to the positive x-axis) is given as

$$H_0(x,y) = e^{ik_0 n_1 (\cos\theta x + \sin\theta y)} = e^{in_1 (k_x x + k_y y)}. \tag{2.76}$$

Looking at Equation (2.37), the $\mathbf{A}^{(k)}$ and $\mathbf{B}^{(k)}$ matrices remains unchanged, while $\mathbf{C}^{(k)}$ and $\vec{b}^{(k)}$, the two contributions coming from the surface integral, changes.

Looking at Equation (2.35), with a field given as $H(x,y) = H_0 + Ae^{in_1k_xx}e^{\pm in_1k_yy}$

$$\begin{aligned}
&\oint \hat{n} \cdot \left(w(x,y)\frac{1}{\epsilon}\nabla H(x,y) \right) dl \\
&= \oint \Big(\hat{n} \cdot w(\hat{y}(-ik_yn_1H_0 \pm ik_yn_1Ae^{in_1k_xx}e^{\pm in_1k_yy}) \\
&\quad + \hat{x}(ik_xn_1H_0 + ik_xn_1Ae^{in_1k_xx}e^{\pm in_1k_yy})) \Big) dl \\
&= \oint \mp ik_yn_1w(x,y)H_0(x,y) + ik_yn_1w(x,y)(H(x,y) - H_0(x,y))dl \\
&= \oint -ik_yn_1w(x,y)H_0(x,y)(1 \pm 1)dl + \oint ik_yn_1w(x,y)H(x,y)dl, \qquad (2.77)
\end{aligned}$$

it can be seen that k_0 simply has to be changed to k_y in $\mathbf{C}^{(k)}$ and $\vec{b}^{(k)}$ to account for the angle. For the boundary conditions, the field can no longer be assumed to be the same along both edges of the structure. However, the field along one edge is given as the field along the other edge, multiplied by the appropriate Bloch function,

$$H(x = -\frac{d}{2}, y) = H(x = \frac{d}{2}, y)e^{ik_xd}. \qquad (2.78)$$

Finally, the reflectance and transmittance coefficients are slightly different when the angle is considered, as the propagation along the x-axis has to be added. These are now given as

$$r = (H(x,y) - H_0(x,y))\, e^{2in_1k_yy_0}e^{-in_1k_yy}e^{in_1k_xx} \qquad (2.79)$$

$$t = H(x,y)e^{in_1k_yy_0}e^{in_1k_y(y+y_0)}e^{in_1k_xx} \qquad (2.80)$$

2.3.2 S-Polarised Light

A structure like this is highly anisotropic when different polarisations are considered, which means that the effective refractive index might vary greatly depending on the polarisation. In the case of s-polarised light, the electric field will be parallel to the cylinders, and the calculations will therefore use the electric field

instead of the magnetic field. The wave equation for the electric field is given as

$$\left(\nabla^2 + \epsilon k^2\right) E(x,y) = 0 \tag{2.81}$$

Using the same approach as for p-polarised light, we get the following integral

$$\begin{aligned} 0 &= \int w(x,y) \left(\nabla^2 + \epsilon k_0^2\right) H(x,y) dydx \\ &= \int \nabla \cdot (w(x,y) \nabla H(x,y)) - \int \nabla w(x,y) \cdot (\nabla H(x,y))\, dydx \\ &+ \int w(x,y) \epsilon k_0^2 H(x,y) dydx \end{aligned} \tag{2.82}$$

From this it can be seen that $\mathbf{A}^{(k)}$, $\mathbf{C}^{(k)}$ and $\vec{b}^{(k)}$ is no longer multiplied by a factor of $\frac{1}{\epsilon^{(k)}}$, while $\mathbf{B}^{(k)}$ is now multiplied by a factor of $\epsilon^{(k)}$. The periodic boundary condition, as well as the calculations of the reflectance and transmittance coefficients remains unchanged when changing to s-polarised light.

2.4 Scattering of Light by a Cylinder

With the effective medium parameters determined, the scattering by a metamaterial might be significantly simplified by considering the metamaterial as a bulk. In this section two approaches to calculating the field will be explored, one using the wave equation for the total field as a basis, and one using the wave equation for the scattered field as a basis. The structure is illustrated in Figure 2.3.

2.4.1 Total Field as Basis

The scattering from a cylinder might be calculated in a similar fashion to how the reflected and transmitted light was calculated for a metamaterial. The calculations in this subsection were made with help from [10]. Considering the

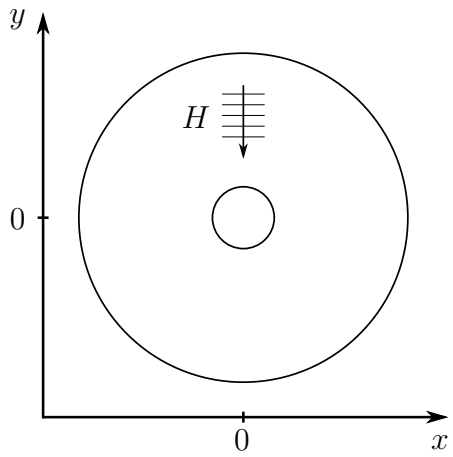

Figure 2.3: A model of the structure considered in this section.

wave equation

$$\left(\nabla\frac{1}{\epsilon}\nabla + k_0^2\right) H(x,y) = 0 \tag{2.83}$$

and using the Galerkin approach, with the same changes described in Equation (2.34) and Equation (2.32), gives

$$\begin{aligned} &-\int \nabla w(x,y)\cdot\left(\frac{1}{\epsilon}\nabla H(x,y)\right) dydx + \int w(x,y)k_0^2 H(x,y)dydx \\ &+\oint \hat{n}\cdot\left(w(x,y)\frac{1}{\epsilon}\nabla H(x,y)\right) dl = 0. \end{aligned} \tag{2.84}$$

The area integrals, which yield $\mathbf{A}^{(k)}$ and $\mathbf{B}^{(k)}$ in Equation (2.37) remains unchanged, while the curve integral, which yields $\mathbf{C}^{(k)}$ and $\vec{b}^{(k)}$ are changed due to different boundary conditions and a change in the structure. For the case of scattering from a cylinder, the total field at a large distance from the cylinder can be expressed as

$$H(x,y) \approx H_0(x,y) + A(\theta)\frac{e^{ik_0 n_1 r}}{\sqrt{r}}, \tag{2.85}$$

where $A(\theta)$ is some function giving the amplitude of the scattered field as a function of the angle, and r is the distance from the cylinder. For an incident field on the

form

$$H_0(x,y) = e^{in_1(k_x x + k_y y)}, \tag{2.86}$$

the integrand for the curve integrals at the boundary can be rewritten as

$$\frac{1}{\epsilon} w(x,y)\hat{n}\cdot\nabla H(x,y) \approx \frac{1}{\epsilon} w(x,y)\hat{r}\cdot\nabla H_0(x,y) + \frac{1}{\epsilon} w(x,y)A(\theta)\left(ik_0 n_1 - \frac{1}{2r}\right)\frac{e^{ik_0 n_1}}{\sqrt{r}} \tag{2.87}$$

$$\approx \frac{1}{\epsilon} w(x,y) ik_0 n_1 \left(\cos\theta\cos\phi + \sin\theta\sin\phi\right) H_0(x,y) \tag{2.88}$$

$$+ \frac{1}{\epsilon} w(x,y)\left(ik_0 n_1 - \frac{1}{2r}\right)\left(H(x,y) - H_0(x,y)\right), \tag{2.89}$$

where ϕ is the angle of $\hat{r}$ relative to the x-axis, and θ is the angle of the incident field (or more accurately, the angle of the wave vector), relative to the x-axis. The integral over the term containing $H(x,y)$ will be the $\mathbf{C}^{(k)}$ contribution, and the integral over the terms containing $H_0(x,y)$ will be the $\vec{b}^{(k)}$ contribution. Using the basis functions described in Equation (2.9) as the weight functions, $\mathbf{C}^{(k)}$ and $\vec{b}^{(k)}$ are given by

$$C_{i,j}^{(k)} = \frac{1}{\epsilon}\left(ik_0 n_1 - \frac{1}{2r}\right)\oint f_i(x,y) f_j(x,y) dl \tag{2.90}$$

$$\begin{aligned} b_i^{(k)} &= \oint f_i(x,y)\frac{1}{\epsilon}\left(\hat{r}\cdot\nabla H_0(x,y) - \left(ik_0 n_1 - \frac{1}{2r}\right)H_0(x,y)\right) dl \\ &= \oint f_i(x,y)\frac{1}{\epsilon}\left(\cos\phi k_x + \sin\phi k_y - \left(ik_0 n_1 - \frac{1}{2r}\right)\right) H_0(x,y) dl \end{aligned} \tag{2.91}$$

From this it can be seen that $\mathbf{C}^{(k)}$ can be calculated in the same way as before, while $\vec{b}^{(k)}$ needs some assumptions on $H_0(x,y)$ along the curve. As the length of the curve is much smaller than the wavelength, the exponential will only change slightly along the curve. This means that the field might be approximated reasonably well as a linear function along the curve,

$$H(\vec{p}) = H_1 + \frac{H_2 - H_1}{l}\vec{p}, \tag{2.92}$$

where H_1 and H_2 are the field at the start end the end of the curve, and p is some point on the curve. Approximating the angle ϕ as constant along the curve, $\vec{b}^{(k)}$ is given by

$$b_i^{(k)} = \frac{1}{\epsilon}\left(\cos\phi k_x + \sin\phi k_y - \left(ik_0 n_1 - \frac{1}{2r}\right)\right) \oint f_i(\vec{p}) H(\vec{p}) dl. \tag{2.93}$$

The integral calculated along the unit curve, with a unit function which goes from 0 to 1 along the curve, can be calculated as

$$\begin{aligned} \oint f_i(\vec{p}) H(\vec{p}) dl &= l \int_0^1 p(H_1 + (H_2 - H_1)p) dp \\ &= l \left[\frac{1}{2} H_1 p^2 + \frac{1}{3}(H_2 - H_1)p^3\right]_0^1 \\ &= l \frac{2H_1 + H_2}{6}, \end{aligned} \tag{2.94}$$

The integral using the other unit function, which goes from 1 to 0 along the curve, will yield the same result with H_1 and H_2 switched around. The last unit function will be 0 along the curve, so that integral will also be zero. With this, $\vec{b}^{(k)}$ is given as

$$\vec{b}^{(k)} = \frac{1}{\epsilon}\left(\cos\phi k_x + \sin\phi k_y - \left(ik_0 n_1 - \frac{1}{2r}\right)\right) \frac{l}{6} \begin{bmatrix} 2H_1 + H_2 \\ H_1 + 2H_2 \\ 0 \end{bmatrix}, \tag{2.95}$$

if the first to vertices are the ones placed on the curve, with the first vertex placed at the start of the curve, and the second vertex placed at the end of the curve. $\mathbf{A}^{(k)}$, $\mathbf{B}^{(k)}$, $\mathbf{C}^{(k)}$ and $\vec{b}^{(k)}$ can be combined in the same way as described in section 2.3 to give the total field at all points. To get only the scattered field at all points, the incident field can be subtracted at each point.

2.5 Scattered Field as Basis

Instead of calculating the scattered field by considering the wave equation for the total field, the scattered field could be calculated by considering only the wave equation of the scattered field. Beginning with the wave equation for the total field, and allowing the permeability to be different from 1, which might be relevant for metamaterials, yields

$$\left(\nabla \frac{1}{\epsilon(x,y)} \nabla + \mu(x,y) k_0^2\right) H(x,y) = 0. \tag{2.96}$$

To express the wave equation in terms of the scattered field, the permittivity and permeability are expressed as

$$\frac{1}{\epsilon(x,y)} = \frac{1}{\epsilon_{ref}(x,y)} + \frac{1}{\epsilon(x,y)} - \frac{1}{\epsilon_{ref}(x,y)}, \tag{2.97}$$

$$\mu(x,y) = \mu_{ref}(x,y) + \mu(x,y) - \mu_{ref}(x,y), \tag{2.98}$$

where $\epsilon_{ref}(x,y)$ and $\mu_{ref}(x,y)$ are the reference permittivity and permeability at a point, i.e. the permittivity and permeability of the material surrounding the scatterers. Dividing Equation (2.96) into a part with the incident field and a part with the scattered field, and using Equation (2.97) and Equation (2.98) in the part with the incident field gives

$$\left(\nabla \frac{1}{\epsilon(x,y)} \nabla + \mu(x,y) k_0^2\right) H_{sct}(x,y) + \underbrace{\left(\nabla \frac{1}{\epsilon_{ref}(x,y)} \nabla + \mu_{ref}(x,y) k_0^2\right) H_0(x,y)}_{0}$$

$$+ \left(\nabla \left(\frac{1}{\epsilon(x,y)} - \frac{1}{\epsilon_{ref}(x,y)}\right) \nabla + \left(\mu(x,y) - \mu_{ref}(x,y)\right) k_0^2\right) H_0(x,y) = 0, \tag{2.99}$$

Arranging Equation (2.99) so that the terms with the scattered field is on one side, and the terms with the incident field is on the other side, and using the Galerkin

approach as demonstrated in the previous sections gives

$$\begin{aligned}
&\int_A w(x,y)\nabla\cdot\frac{1}{\epsilon(x,y)}\nabla H_{sct}(x,y)dA+\int_A w(x,y)\mu(x,y)k_0^2H_{sct}(x,y)dA\\
=&-\int_A w(x,y)\nabla\cdot\left(\left(\frac{1}{\epsilon(x,y)}-\frac{1}{\epsilon_{ref}(x,y)}\right)\nabla H_0(x,y)\right)dA\\
&-\int_A w(x,y)(\mu(x,y)-\mu_{ref}(x,y))k_0^2H_0(x,y)dA
\end{aligned}\tag{2.100}$$

The terms on the left hand are on the same form as in Equation (2.32), except that the second term now includes the permeability. As the permeability is considered to be constant in the triangle, and thereby constant over the integral, this simply results in a factor of $\mu^{(k)}$ in the integral, and so the matrices $\mathbf{A}^{(k)}$ and $\mathbf{B}^{(k)}$ can be calculated in a similar fashion. This means that it is only the terms on the right hand side that is significantly different. For the first term, the integrand can be rewritten using

$$\begin{aligned}
&\nabla\cdot\left(\left(\frac{1}{\epsilon(r)}-\frac{1}{\epsilon_{ref}(r)}\right)\nabla H_0(x,y)\right)\\
=&\left(\nabla\left(\frac{1}{\epsilon(r)}-\frac{1}{\epsilon_{ref}(r)}\right)\right)\cdot\nabla H_0(x,y)+\left(\frac{1}{\epsilon(r)}-\frac{1}{\epsilon_{ref}(r)}\right)\nabla^2H_0(x,y),
\end{aligned}\tag{2.101}$$

which gives the two integrals

$$\begin{aligned}
&-\int_A w(x,y)\nabla\cdot\left(\left(\frac{1}{\epsilon(x,y)}-\frac{1}{\epsilon_{ref}(x,y)}\right)\nabla H_0(x,y)\right)dA\\
=&-\int_A w(x,y)\nabla\left(\frac{1}{\epsilon(x,y)}-\frac{1}{\epsilon_{ref}(x,y)}\right)\cdot\nabla H_0(x,y)dA\\
&-\int_A w(x,y)\left(\frac{1}{\epsilon(x,y)}-\frac{1}{\epsilon_{ref}(x,y)}\right)\nabla^2H_0(x,y)dA
\end{aligned}\tag{2.102}$$

The second integral on the right hand side is the simplest to calculate. The Laplace operator working on the incident field is given as

$$\nabla^2H_0(x,y)=-k_0^2\epsilon H_0(x,y).\tag{2.103}$$

Approximating the field to be constant throughout the triangle, with its value given as the value in the centre of the triangle, as well as using the unit functions Equation (2.9) as the weight functions gives

$$\begin{aligned}
&-\int_A w(x,y)\left(\frac{1}{\epsilon(x,y)}-\frac{1}{\epsilon_{ref}(x,y)}\right)\nabla^2 H_0(x,y)dA \\
=&k_0^2\epsilon\left(\frac{1}{\epsilon(x,y)}-\frac{1}{\epsilon_{ref}(x,y)}\right)H_0(\tilde{x},\tilde{y})\sum_{i=1}^{3}\int_A f_i(x,y)\vec{a}_i dA \\
=&k_0^2\epsilon\left(\frac{1}{\epsilon(x,y)}-\frac{1}{\epsilon_{ref}(x,y)}\right)\frac{A^{(k)}}{3}H_0(\tilde{x},\tilde{y})\sum_{i=1}^{3}\vec{a}_i, \qquad (2.104)
\end{aligned}$$

where $\tilde{x},\tilde{y}$ are the value of x and y at the centre. The last equality comes from the fact that the integral of one of the unit functions over a triangle is simply one third of the area of the triangle. To calculate the first integral in Equation (2.102), the integrand has to be rewritten. The part in the parentheses is a step function, and the gradient of a step function can be evaluated as

$$U(x,y) = U_1 + (U_2-U_1)\Theta\left(x-x_0(y), y-y_0(x)\right) \qquad (2.105)$$

$$\begin{aligned}
\hat{x}\frac{dU}{dx}+\hat{y}\frac{dU}{dy} &= \left(\hat{x}\frac{dy_0(x)}{dx}+\hat{y}\frac{dx_0(y)}{dy}\right)(U_2-U_1)\delta(x-x_0(y),y-y_0(x)) \\
&= \hat{n}(U_2-U_1)\delta(x-x_0(y),y-y_0(y)), \qquad (2.106)
\end{aligned}$$

where Θ is the unit step function and δ is the Dirac Delta function. Inserting Equation (2.106) into the integral yields

$$\begin{aligned}
&-\int_A w(x,y)\nabla\left(\frac{1}{\epsilon(x,y)}-\frac{1}{\epsilon_{ref}(x,y)}\right)\cdot\nabla H_0(x,y)dA \\
=&-\left(\left(\frac{1}{\epsilon_2}-\frac{1}{\epsilon_{ref2}}\right)-\left(\frac{1}{\epsilon_1}-\frac{1}{\epsilon_{ref1}}\right)\right)\int_A w\hat{n}\cdot\nabla H_0(x,y)\delta(x-x_0(y),y-y_0(y))dA, \qquad (2.107)
\end{aligned}$$

where ϵ_2 and $\epsilon_{ref,2}$ is the permittivity and the reference permittivity of the triangle the normal vector is pointing to, and ϵ_1 and $\epsilon_{ref,1}$ is the permittivity and the reference permittivity of the triangle the normal vector is pointing away from.

As the integrand is only non-zero along the edge of the scatterer, this can be converted into a curve integral along that edge. Using the unit functions as the weight functions, and using the field at the centre of the line as the value for the incident field gives

$$\begin{aligned} &-\int_A w(x,y)\nabla\left(\frac{1}{\epsilon(x,y)}-\frac{1}{\epsilon_{ref}(x,y)}\right)\cdot\nabla H_0(x,y)dA \\ &\approx -\left(\left(\frac{1}{\epsilon_2}-\frac{1}{\epsilon_{ref2}}\right)-\left(\frac{1}{\epsilon_1}-\frac{1}{\epsilon_{ref1}}\right)\right)(n_x\cos\theta+n_y\sin\theta)H_0(\tilde{x},\tilde{y})\sum_{i=1}^{3}\int_l f_i(x,y)\vec{a}_i dl, \end{aligned} \tag{2.108}$$

where n_x and n_y are the x and y components of the normal vector. For the vertices that is on the edge of the scatterer, the curve integral over the unit function is simply half the edge length, while it is zero for a vertex that is not on the edge. The only remaining term to calculate is the last integral on the right hand side in Equation (2.100). Using an incident field that is constant over the triangle, and using the unit functions as the weigth functions, and remembering that integrating a unit function over a triangle gives one third of the area, the integral can be expressed as

$$\begin{aligned} &-\int_A w(x,y)(\mu(x,y)-\mu_{ref}(x,y))k_0^2 H_0(x,y)dA \\ &\approx -\frac{A^{(k)}}{3}(\mu(x,y)-\mu_{ref}(x,y))k_0^2 H_0(\tilde{x},\tilde{y})\sum_{i=1}^{3}\vec{a}_i. \end{aligned} \tag{2.109}$$

Combining these terms gives a matrix equation of the form

$$\left(-\mathbf{A}^{(k)}+\mathbf{B}^{(k)}\right)\begin{bmatrix} a_1^{(k)} \\ a_2^{(k)} \\ a_3^{(k)} \end{bmatrix} = \begin{bmatrix} b_1^{(k)} \\ b_2^{(k)} \\ b_3^{(k)} \end{bmatrix}, \tag{2.110}$$

where the matrices are given as

$$A_{i,j}^{(k)} = \frac{1}{\epsilon_k} \int \nabla f_i(u,v) \cdot \nabla f_j(u,v) dxdy, \tag{2.111}$$

$$B_{i,j}^{(k)} = \mu_k k_0^2 \int f_i(u,v) f_j(u,v) dxdy \tag{2.112}$$

and the vector $\vec{b}$ is the sum of Equation (2.104),Equation (2.108) and Equation (2.109),

$$\begin{aligned} b_i^{(k)} =& k_0^2 \epsilon \left(\frac{1}{\epsilon(x,y)} - \frac{1}{\epsilon_{ref}(x,y)} \right) \frac{A^{(k)}}{3} H_0(\tilde{x},\tilde{y}) \\ & - \left(\left(\frac{1}{\epsilon_2} - \frac{1}{\epsilon_{ref2}} \right) - \left(\frac{1}{\epsilon_1} - \frac{1}{\epsilon_{ref1}} \right) \right) (n_x \cos\theta + n_y \sin\theta) H_0(\tilde{x},\tilde{y}) \int_l f_i(x,y) \\ & - \frac{A^{(k)}}{3} (\mu(x,y) - \mu_{ref}(x,y)) k_0^2 H_0(\tilde{x},\tilde{y}) \end{aligned} \tag{2.113}$$

Solving this matrix equation for each triangle, and combining the solutions as described in Equation (2.68) gives the scattered field throughout the structure. However, as the structure has to end somewhere, the edges of the structure will serve as some artificial barrier, which will reflect the field. To avoid this problem, a perfectly matched layer can be added to the edge of the structure to absorb the field, so that there is practically no field that gets reflected. This is done by redefining the field as

$$H_{sct,pml} = H_{sct} e^{-\sigma(r)}, \tag{2.114}$$

where r is the distance from the centre of the scatterer. This is equivalent to multiplying the exponent of H_{sct} by a factor $(1 + i\sigma)$. $\sigma(r)$ should be defined as

$$\sigma(r) = \begin{cases} 0, & \text{for } r < r_{pml} \\ \sigma_0 (r - r_{pml})^2 & \text{for } r < r_{pml}, \end{cases} \tag{2.115}$$

where r_{pml} is the distance from the scatterer at which the PML starts, and σ_0 is a coefficient which has to be determined. Applying this ensures that the scattered

field decreases exponentially in the PML zone. This means that the PML has to be placed at a sufficiently large radius, as the scattered field will not be accurately depicted in this area. σ_0 should be chosen so that it is large enough that the scattered field practically vanishes in the PML, while still being small enough that the PML surface does not cause reflection. To achieve this balance, the thickness of the PML layer also has to be adjusted. In terms of the matrix elements, this will affect $\mathbf{A}$, where the derivative of the field appears, and this will result in $\mathbf{A}$ having to be multiplied by a factor of $(1+i\sigma)^{-2}$. The total field can be calculated by adding the incident field at each point.

2.5.1 Scatterer on a Surface

Now that a method for calculating the scattered field from a free scatterer has been described, the method could be adapted to calculate the field scattered by a scatterer placed on some surface. Assuming that the surface is parallel to the x-axis, and placed at a height $y = 0$, the reference field is given as

$$E_0(r) = \begin{cases} E_0(e^{ik_0 n_1(\cos\theta x + \sin\theta y)} + re^{ik_0 n_1(\cos\theta x - \sin\theta y)}) & y > 0 \\ E_0 te^{ik_0 n_2(\cos\theta' x + \sin\theta' y)} & y < 0, \end{cases} \tag{2.116}$$

where r and t are the reflectance and transmittance coefficients and θ and θ' are the angles of the light above and below the surface. The calculations with the added surface are very similar to the calculations without the surface, the only thing that changes is that the appropriate expression for the reference field has to be selected, based on whether the triangle is above or below the surface, as no triangle will be placed across the surface. The reflectance- and transmittance coefficients are given by the Fresnel equations [11]

$$r_s = \frac{n_1\cos\theta - n_2\cos\theta'}{n_1\cos\theta + n_2\cos\theta'} \quad t_s = \frac{2n_1\cos\theta}{n_1\cos\theta + n_2\cos\theta'} \tag{2.117}$$

$$r_p = \frac{n_2\cos\theta - n_1\cos\theta'}{n_2\cos\theta + n_1\cos\theta'} \quad t_p = \frac{2n_1\cos\theta}{n_2\cos\theta + n_1\cos\theta'}, \tag{2.118}$$

where r_s and t_s are the reflectance and transmittance coefficients for s-polarised light, and r_p and t_p are the reflectance and transmittance coefficients for p-polarised light. Note that these coefficients depend on the way the field is defined, and may have opposite sign for field defined in another way.

2.5.2 S-Polarised Light

When the permeability is considered, the wave equation for the electric field is given as

$$\left(\nabla \frac{1}{\mu(x,y)} \nabla + \epsilon(x,y) k_0^2\right) E(x,y) = 0. \tag{2.119}$$

From this it can be seen that the equations for the s-polarised light is the same as the equations for the p-polarised light, where the permeability and the permittivity has been exchanged, and the electric field is considered instead of the magnetic field. This means that the approach described above can be used with very few changes. It should be noted that when the reference field is calculated in the case of a scatterer on a surface, the reflectance and transmittance coefficient are used, which depends on the polarisation.

2.6 Effective Medium Theory

Effective medium theory is about treating some composite material as a bulk material by assigning some effective parameters, such as an effective refractive index. If these effective parameters can be assigned to the material, many calculations, such as the scattering of light by a material, can be significantly simplified, as the composite material can now be considered a bulk material. In this section the focus will be on assigning an effective refractive index and effective impedance, and using these values to calculate an effective permittivity and permeability. There are different approaches to calculating the effective parameters. One of the simplest approaches, as suggested by [12], is taking some weighted average of the

parameters of the composite materials,

$$n_{eff} = f_1 n_1 + f_2 n_2 + ... + f_k n_k, \tag{2.120}$$

where f_i is the filling factor of the i'th material, and n_i is the refractive index of the i'th material. This approach does not consider the structure of the metamaterial, which implies that the method might not work well for metamaterials where the structure plays a significant role. For materials consisting of some bulk materials containing some randomly distributed particles of another material, or maybe a structure consisting of layers of different materials, this method might be effective. Alternatively, the effective refractive index could be calculated by considering the reflectance and transmittance coefficients.

For light with normal incidence, these can be calculated analytically for a bulk material, using the reflection and transmission coefficients of the interfaces. For the reflection, the following sum is considered:

$$\begin{aligned} r =& r_{12} + t_{12}e^{\alpha}r_{21}e^{\alpha}t_{21} + t_{12}e^{\alpha}r_{21}e^{\alpha}r_{21}e^{\alpha}r_{21}e^{\alpha}t_{21} + ... \\ =& r_{12} + t_{12}r_{21}^{-1}t_{21}\sum_{j=1}^{\infty}\left(r_{21}^2 e^{2\alpha}\right)^j \\ =& r_{12} + \frac{t_{12}r_{21}t_{21}e^{2\alpha}}{1 - r_{21}^2 e^{2\alpha}}, \end{aligned} \tag{2.121}$$

where r_{12} and r_{21} refers to reflection in area 1 and area 2 respectively, and t_{12} and t_{21} refers to transmission from area 1 to area 2, and from area 2 to area 1 respectively, and $\alpha = ik_0nd$, where n is the effective refractive index of the material and d is the thickness. Similarly, the transmission can be calculated,

$$\begin{aligned} t =& t_{12}e^{\alpha}t_{21} + t_{12}e^{\alpha}r_{21}e^{\alpha}r_{21}e^{\alpha}t_{21} + t_{12}e^{\alpha}r_{21}e^{\alpha}r_{21}e^{\alpha}r_{21}e^{\alpha}r_{21}e^{\alpha}t_{21} + ... \\ =& t_{12}e^{\alpha}t_{21}\sum_{j=0}^{\infty}\left(r_{21}^2 e^{2\alpha}\right)^j \\ =& \frac{t_{12}e^{\alpha}t_{21}}{1 - r_{21}^2 e^{2\alpha}}. \end{aligned} \tag{2.122}$$

The expressions for r and t can be rewritten using the relations

$$\begin{aligned} r_{12} =& - r_{21} && (2.123)\\ t_{12} =& 1 - r_{12} && (2.124)\\ t_{21} =& 1 - r_{21} = 1 + r_{12} && (2.125)\\ t_{12}t_{21} =& 1 - r_{12}^2 && (2.126) \end{aligned}$$

The goal is to express r and t in term of r_{12} only. Starting with r,

$$\begin{aligned} r =& \frac{r_{12}(1 - r_{12}^2 e^{2\alpha})}{(1 - r_{12}^2 e^{2\alpha})} + \frac{r_{12}(r_{12}^2 - 1)e^{2\alpha}}{(1 - r_{12}^2 e^{2\alpha})} \\ =& \frac{r_{12} - r_{12}e^{2\alpha}}{(1 - r_{12}^2 e^{2\alpha})}, \end{aligned} \tag{2.127}$$

and similarly for t,

$$t = \frac{(1 - r_{12}^2)e^{\alpha}}{1 - r_{12}^2 e^{2\alpha}} \tag{2.128}$$

Equation (2.127) can be used to express r_{12} in term of a quadratic equation,

$$\begin{aligned} r(1 - r_{12}^2 e^{2\alpha}) &= r_{12} - r_{12}e^{2\alpha} \\ -re^{2\alpha}r_{12}^2 + r_{12}(e^{2\alpha} - 1) + r &= 0 \\ r_{12} = \frac{-(e^{2\alpha} - 1) \pm \sqrt{(e^{2\alpha} - 1)^2 + 4r^2e^{2\alpha}}}{-2re^{2\alpha}}&. \end{aligned} \tag{2.129}$$

The same can be done using Equation (2.128),

$$\begin{aligned} t(1 - r_{12}^2 e^{2\alpha}) &= (1 - r_{12}^2)e^{\alpha} \\ (e^{\alpha} - te^{2\alpha})r_{12}^2 + t - e^{\alpha} &= 0 \\ r_{12} = \frac{\pm\sqrt{-4(e^{\alpha} - te^{2\alpha})(t - e^{\alpha})}}{2(e^{\alpha} - te^{2\alpha})}&. \end{aligned} \tag{2.130}$$

Subtracting Equation (2.130) from Equation (2.129) gives

$$0 = \frac{-(e^{2\alpha}-1) \pm \sqrt{(e^{2\alpha}-1)^2 + 4r^2e^{2\alpha}}}{-2re^{2\alpha}} - \frac{\pm\sqrt{-4(e^{\alpha}-te^{2\alpha})(t-e^{\alpha})}}{2(e^{\alpha}-te^{2\alpha})} = f(n), \tag{2.131}$$

as α is a function of n. Finding the value for n where $f(n)$ gives 0 gives the value of the effective refractive index. While this may not be done analytically, it can be done numerically. Since $f(n)$ gives a complex number, the phase of f can be calculated. At $f(n) = 0$, the phase will be undefined, which leads to a phase singularity at this point. By dividing the complex plane into rectangles, the phase singularity can be found be calculating the phase change along each edge of each rectangle. The rectangle containing the singularity should have a large jump in phase along only one edge. Once the rectangle containing the singularity has been found, the location of the singularity can be more accurately determined by dividing the rectangle into smaller rectangles, and repeating the process, until a satisfying accuracy has been achieved.

Alternatively, the approach presented in [13] and [14], could be applied, however this approach requires more work in analysing the data. By considering the relations between the reflectance and transmittance coefficients and the refractive index and impedance,

$$\frac{1}{t} = \left(\cos(nkd) - \frac{i}{2}\left(Z + \frac{1}{Z}\right)\sin nkd\right)e^{ikd} \tag{2.132}$$

$$\frac{r}{t'} = -\frac{i}{2}\left(Z - \frac{1}{Z}\right)\sin nkd, \tag{2.133}$$

where t is the transmittance, t' is what the article refers to as the normalised transmittance, r is the reflectance, n is the refractive index, k is the wavenumber, d is the thickness of the material and Z is the impedance [13]. Note that the normalised transmittance is simply referred to as the transmittance coefficient in this report, and the relation between the transmittance and normalised transmittance is $t' = te^{ikd}$. Inverting these equations to isolate for the refractive index and

impedance yields [13]

$$Re(n) = \pm\frac{1}{kd}Re\left(\cos^{-1}\left(\frac{1}{2t'}\left(1-\left(r^2-t'^2\right)\right)\right)\right)+\frac{2\pi m}{kd}, \quad m\in\mathbb{N} \tag{2.134}$$

$$Im(n) = \pm\frac{1}{kd}Im\left(\cos^{-1}\left(\frac{1}{2t'}\left(1-\left(r^2-t'^2\right)\right)\right)\right) \tag{2.135}$$

$$Z = \pm\sqrt{\frac{(1+r)^2-t'^2}{(1-r)^2-t'^2}}. \tag{2.136}$$

These equations presents a couple of ambiguities, namely the sign of the expressions and the "branch" of the real component of the refractive index, determined by m. Assuming that the matematerial is a passive material, the problem with the sign can be resolved by demanding that the real component of the impedance and the imaginary component of the refractive index are non-negative. This requirement also gives the sign of the real component of the refractive index, which has to use the same sign as the imaginary component, as the two equations come from the same equation. All that remains is to determine the correct branch of the real component of the refractive index. In [13] the branch is determined by calculating the reflectance and transmittance coefficients for different thicknesses of the material, and demanding that the refractive index does not depend on the thickness. Since the distance between the branches increases as the material's thickness decreases, it is easiest to determine the correct branch for small thicknesses.

Another problem when determining the effective medium parameters is that the edges of the metamaterial might not be well defined, as this will effect the material thickness, which is used for the calculation. In the case of a periodic metamaterial which is created by repeating some unit rectangle, [14] suggests that the effective edges of the metamaterial might be found by starting with the edges of the first and last unit rectangle, which is then displaced by the lengths l_1 and l_2 respectively. The set l_1, l_2 is determined by minimising the difference in the impedance for two different thicknesses at various wavelengths, i.e. the values

that minimises

$$f(l_1, l_2) = \frac{1}{N_\lambda} \sum_{i=1}^{N_\lambda} \frac{|z_1(\lambda_i, l_1, l_2) - z_2(\lambda_i, l_1, l_2)|}{max\left(|z_1(\lambda_i, l_1, l_2)|, |z_2(\lambda_i, l_1, l_2)|\right)}, \tag{2.137}$$

where N_λ is the number of sample wavelengths, and z_1 and z_2 are the impedance calculated for a different number of unit rectangles. In [14] the displacement lengths are limited to half the length of a unit rectangle.

3

Implementation

The point of this chapter is to cover, in very general terms, some of the steps taken in the creation of the script. Specific examples are shown in an attempt to clarify the implementation method.

Having finished the analytic and numerical foundation, the next step is the implementation. A two-dimensional representation of the scatterers which make up the metamaterial is used. For these scatterers, two shapes are chosen: completely circular or square with rounded corners.
As professed in the introduction, the chosen numerical method is the FEM. As such, the produced structures and situations are tessellated into a mesh of triangles of variable sizes. The numerical calculations relate the values of these triangles with one another as explained in Chapter 2.
The implementation of the method was done using the following overall steps:

- Creation of structure.
- Mesh generation.
- Selection of zones.
- Calculation of the scattered field.

3.1 Creation of Structure

The creation of the overall structure one wishes to examine is done by using Constructive Solid Geometry (CSG). The general concept of CSG is to create complicated structures using a combination of simple geometric shapes. The allowed simple shapes, called 'primitives', in two dimensions are circles, polygons, rectangles and ellipses. The advanced structures are created by overlapping primitives and by applying a Set Formula. The Set Formula contains the operations found in set theory, which are the Union ($\cup$), Difference ($-$) or Intersection ($\cap$).
Matlab allows for the creation of primitives using the command line. The Matlab syntax is dependant on the desired primitive. An example of such syntax can be shown in either the creation of a simple circle:

```
geom = [1 , center_x , center_y , radius];
```

or a simple rectangle:

```
geom = [3 , 4 , x1 , x2 , x3 , x4 , y1 , y2 , y3 , y4];
```

The numbers in the first column, 1 and 3, are the indicators of the geometric shape (circle & rectangle), and are simply part of the Matlab syntax.
Figure 3.1 shows a simple example of how CSG works. Figure 3.1(a) shows a square being intersected by a circle. Subtracting the area of the circle from the square yields the situation shown in Figure 3.1(b).
The function `decsg` is then used to decompose the CSG into minimal regions, which are used in the generation of a mesh. Additionally, one can ask `decsg` for a second output, which is an array relating the acquired minimal regions to the original primitives.

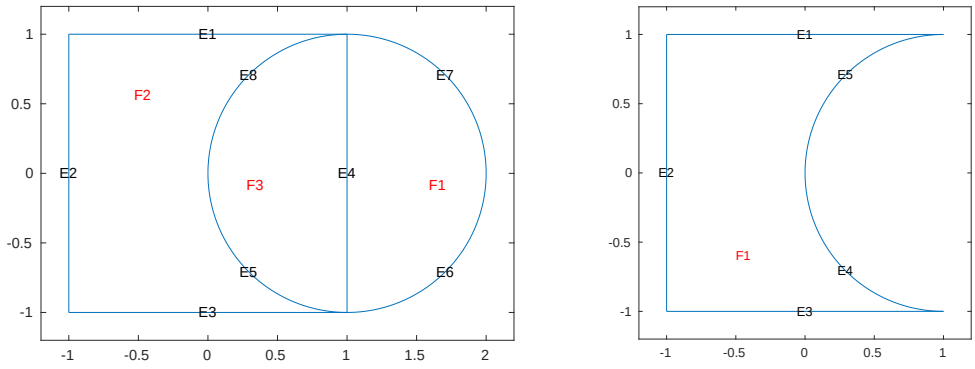

(a) **(b)**

Figure 3.1: *An example of Constructive Solid Geometry. Face and edge labels are shown. (a) A circle overlapping a square. (b) The rectangle with the circle subtracted.*

3.2 Mesh Generation

When the desired structure has been created and the minimal regions have been determined, the generation of a tessellating mesh can be done. A prerequisite to

mesh generation is the creation of a model container. This is simply achieved by using the `createpde` function. To assign the geometric edges obtained in the determination of the minimal regions to the model, one simply has to use the `geometryFromEdges` command. With the model now containing the correct edges, the mesh generation is done by merely using the command `generateMesh` (which has options to increase or decrease the tessellation resolution). The mesh generated by using the edges seen in Figure 3.1(b) yields the mesh seen in Figure 3.2. The information contained in the mesh can be converted for easier

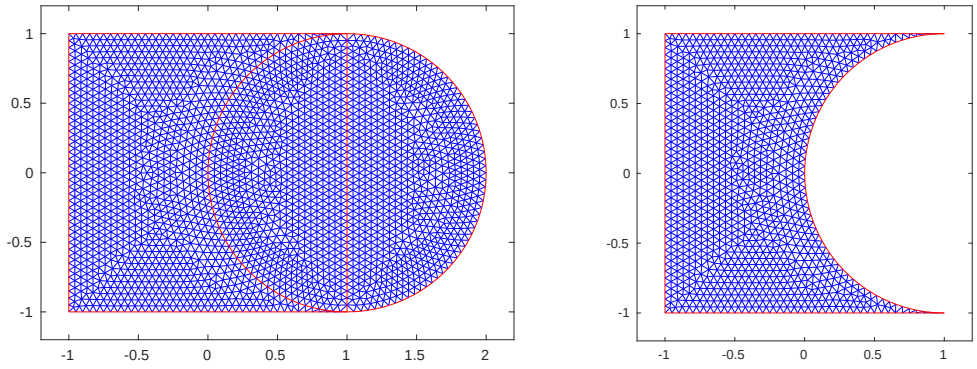

(a) **(b)**

Figure 3.2: *Tesselation of the CSGs found in Figure 3.1 with a* Hmax *of* 0.05.

manipulation. This is done using the command `meshToPet`, and will yield three arrays.

Every column in the `p` array contains the x- and y-coordinates of a single unique point/vertex in the mesh.

The `e` array is more complicated. Every column represents a specific edge, and the content of its rows can be seen in Table 3.1.

The columns of the `t` array correspond to all the triangles in the mesh. The first three rows represent the three points/vertices making up the corners of the triangle, and refer to column indices in the `p` array. The fourth row represents the face in which the triangle resides.

Table 3.1: *The contents of the rows in the* `e` *array.*

Row number	Content
1	Index of first point in mesh edge
2	Index of second point in mesh edge
3	Parameter value of first point
4	Parameter value of second point
5	Edge ID
6	Subdomain on left side of edge
7	Subdomain on right side of edge

3.3 Selection of Zones

The structure in Figure 3.1(b) is very simple, and as can be seen, only one face (area) is present. If one were to instead consider the structure in Figure 3.1(a), one can observe the three faces created by the intersecting lines.
The calculations are done incrementally for all the triangles in the generated mesh. Thus, one must designate which faces correspond to which elements in the structure (e.g. face 1 is the environment, face 2 is the scatterer). Then, using the fourth row in array `t`, one can determine which parameters each of the triangles must adopt.
Unfortunately, Matlab's labelling of the structure's faces is done seemingly randomly. This makes it difficult to program a process which automatically determines whether a face belongs to the environment or to a scatterer.
While technically possible, if one was dealing with many scatterers, the process of manually inputting which faces correspond to which materials would be very tedious. Hence, automation of the process of zone determination is a central part of a generalised script.
The relation array obtained by the `decsg` function seemed like the only way to automate the face determination. The rows of the array represent the faces, while the columns represent the original primitives. The array consists of 0's and 1's. If a certain face is located within the area of a primitive, the number 1 will appear at their corresponding row and column. Using this information in addition to

the information provided by the primitives, one can automatically determine the face-material correspondence up to a certain degree.

3.4 Calculation of the Scattered Field

Having created the mesh as well as knowing which faces correspond to which material, the calculation of the field can now be accomplished. As every element of the mesh has an influence, the chosen numerical approach is the create a for-loop iterating over all the triangles in the mesh. The actual theoretical calculations are covered in Chapter 2.

Depending on the amount of triangles present in the mesh, the $\mathbf{M}$ matrix, which stores all the points' respective values, has the potential to become quite large. For n triangles, the result would be an $n \times n$ $\mathbf{M}$ matrix. It is not inconceivable to have upwards of 50.000 triangles in the mesh, which would result in an $\mathbf{M}$ matrix of 2.5 billion elements. Storing this on a PC would require 18.6 Gigabytes of RAM. Fortunately, many of the elements of the $\mathbf{M}$ matrix consist of 0's. Therefore, a sparse matrix can be used. A sparse matrix does not explicitly store values in the indices which contain 0 values, and thus a lot of space can be saved.

The pre-allocated sparse matrix has values placed inside it at every iteration of the for-loop. The indices in which these values are placed are simply chosen using the information contained in the `t` array of the triangle in the current iteration. As previously stated, the indices of the triangle's three points are located in the first three rows of the `t` matrix. Using the x- and y-values of these points in the calculations, nine values are added to the sparse matrix in indices corresponding to the points' indices in the `p` array. Since many of the points in the mesh are shared between triangles, numerous indices in the sparse matrix are accessed multiple times.

Once the sparse matrix has been filled, it is only a question of dividing the b vector by the $\mathbf{M}$ matrix as shown in Equation (2.68).

4

Results & Discussion

This chapter presents the results gathered with the Matlab scripts. Typically a figure will be presented, followed by a discussion of that figure. The chapter starts with the effective parameters for variations on the structure of the metamaterial. If nothing else is stated, the standard for the metamaterial is gold cylinders with a radius of 12 nm and a period of 30 nm, repeated for 10 rows, and with an s-polarised incident field. Next, the scattering figures is presented, which was calculated using both an array of gold cylinders, and a bulk material with the corresponding effective parameters. These are compared. The chapter ends with a discussion on the scripts that have been created by the authors. Some results were not considered relevant enough to be presented in this chapter are displayed in Appendix A.

Contents

2.1 The Wave Equations 7

2.2 The Finite Element Method 8

2.3 Calculating Reflectance and Transmittance 14

2.4 Scattering of Light by a Cylinder 25

2.5 Scattered Field as Basis 29

2.6 Effective Medium Theory 35

4.1 Effective Parameters

When calculating the effective parameters, it was quickly seen that the method described by Equation (2.131) was not sufficient for the metamaterials that are examined in this section, as that method found multiple singularities, with variations in both the real and imaginary parts of the refractive index. This might be because the expressions used did not account for the impedance, but rather assumed that it was the inverse of the refractive index. This would also imply that the weighted average approach, described by Equation (2.120), would be insufficient. Therefore all the effective parameters presented in this section has been calculated using the method described by Equation (2.134), Equation (2.135) and Equation (2.136)

4.1.1 S-Polarisation

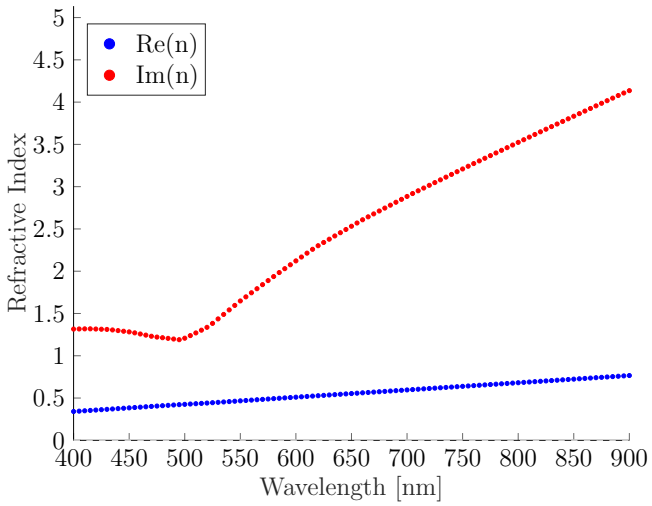

Figure 4.1: The refractive index of a square array of gold cylinders with a radius of 12 nm and a period of 30 nm. The incident field is s-polarised, i.e. the magnetic field component is parallel to the cylinders. The refractive index is calculated for an array of 10 rows thickness.

In Figure 4.1 the effective refractive index of the metamaterial can be seen. The real part is much lower than the imaginary part, and the material is expected to behave metallic. This is consistent with Figure A.1 where it can be seen that

only a small portion of the light passes through the metamaterial. Comparing the effective real refractive index calculated from the reflectance and transmittance coefficients to the weighted average, as seen in Figure 4.2, shows a very poor fit. For the imaginary component, the values calculated from reflectance and transmittance seem to roughly follow the same shape as that of the bulk or weighted average, but the actual value are somewhere between the bulk and weighted average. All the imaginary components shares a bend around 500 nm, followed by a steep increase, but this is less pronounced for the weighted average.

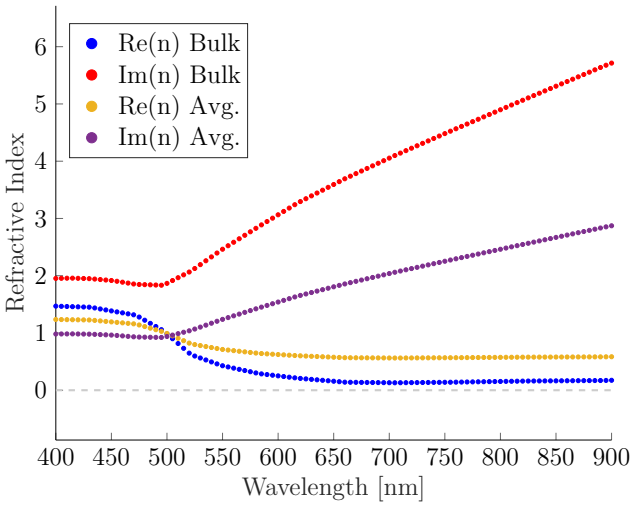

Figure 4.2: The refractive index for bulk gold and the weighed average between the refractive index for gold and air (n=1), using for a material consisting of 50.3% gold. The refractive index of gold is calculated by linear interpolation at the given wavelength, using the data file [ref].

Figure 4.2 depicts the refractive index of gold, as well as the weighted average between gold and air, for a metamaterial with a cylinder radius of 12 nm and a period of 30 nm. This amounts to a roughly even split between air and gold. For air, the refractive index was set to be 1 + 0i for all wavelengths and the refractive index for gold was found from a linear interpolation between the data points in the data file used for the Matlab code. This data file has 15 data points in the spectrum where the refractive index was calculated. The curves seem fairly smooth in the spectrum, so it seems like a linear interpolation gives a sufficiently accurate refractive index. The bulk values was used for the gold cylinders in the script, but as the permittivity and permeability were used instead of the refractive

index, these were set as $\epsilon_{gold} = n_{gold}^2$ and $\mu_{gold} = 1$.

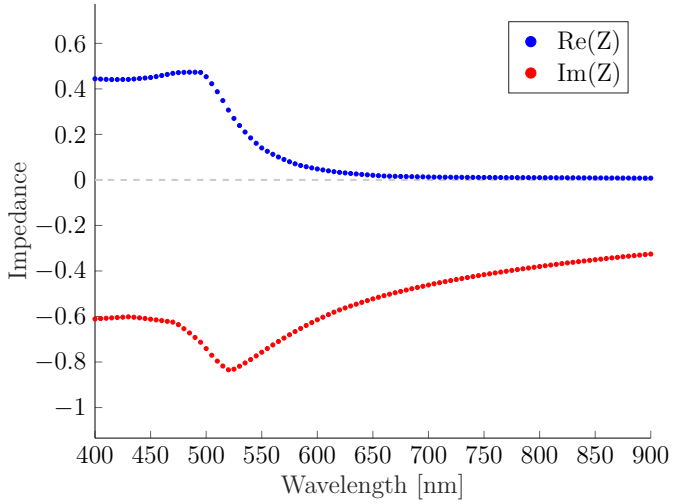

Figure 4.3: The impedance of a square array of gold cylinders with a radius of 12 nm and a period of 30 nm. The incident field is s-polarised. The impedance is calculated for an array of 10 rows thickness.

In Figure 4.3 the impedance of the metematerial is illustrated. A problem with determining the impedance from the reflectance and transmittance coefficients is that the sign of the equation is determined by requiring that the real component is non-negative. Normally this is unambiguous, but if the real component is very close to 0, the sign could be determined by the noise in the calculations, which could lead to the wrong sign for the imaginary component. For the high end of the spectrum, the real part of the impedance in close to zero, but it does not seem to have caused any problems, as the only effect this could have on the imaginary part is to change the sign. As the sign of the imaginary part does not change throughout the spectrum, and the sign must be right for the low end of the spectrum, where the real part is too far away from 0 for the sign to be determined by noise, the sign of the imaginary part must be right throughout the spectrum.

In Figure 4.4 the relative permittivity of the metamaterial can be seen. This is calculated from the effective refractive index and impedance. After a bend abound 500 nm the real component has a steep decline, while the imaginary part is less dependant on the wavelength. It might be interesting to see how this changes beyond the spectrum, but the data for the refractive index of gold, which was

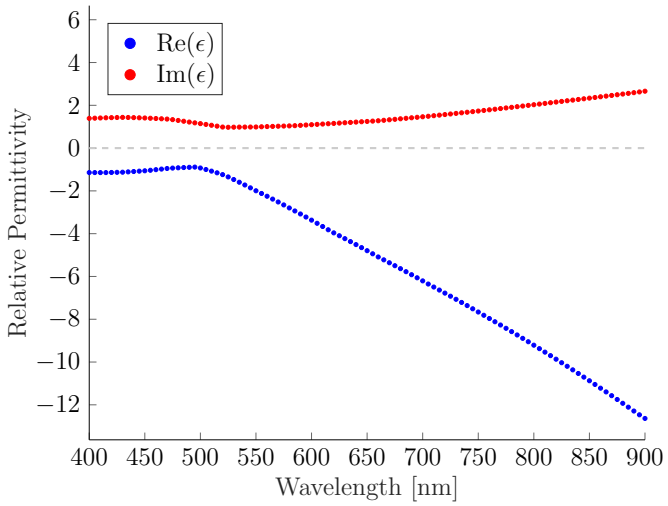

Figure 4.4: The relative permittivity of a square array of gold cylinders with a radius of 12 nm and a period of 30 nm. The incident field is s-polarised. The relative permittivity is calculated for an array of 10 rows thickness. The grey dashed line marks 0 on the y-axis for easier reading.

used for the calculations, starts to become sparse beyond 900 nm, and judging by the values at the data points, a linear interpolation might not be accurate in this region.

In Figure 4.5, the relative permeability for a metamaterial consisting of an array of gold cylinders can be seen. The real part increases from approximately 1 to 1.5 over the spectrum, while the imaginary part goes from positive to negative. For comparison, the relative permeability used for the calculations was 1 + 0i for both gold and air. This means that any method for calculating the effective parameters that used some weighted average, or that does not consider the impedance (implying $Z = 1/n$) would not get the same result for the permeability of the metamaterial. The rate at which the magnetic field and the electric field is dissipated into heat in a material is proportional to the imaginary part of the permeability and permittivity, respectively, which becomes negative if the imaginary parts are negative. For a passive medium, this rate must be non-negative, however, this does not mean that both imaginary parts has to be positive, but simply that both cannot be negative at the same time. As the imaginary part of the permittivity remains positive throughout the spectrum, having a negative imaginary part for the permeability is not necessarily a problem for a passive medium [15].

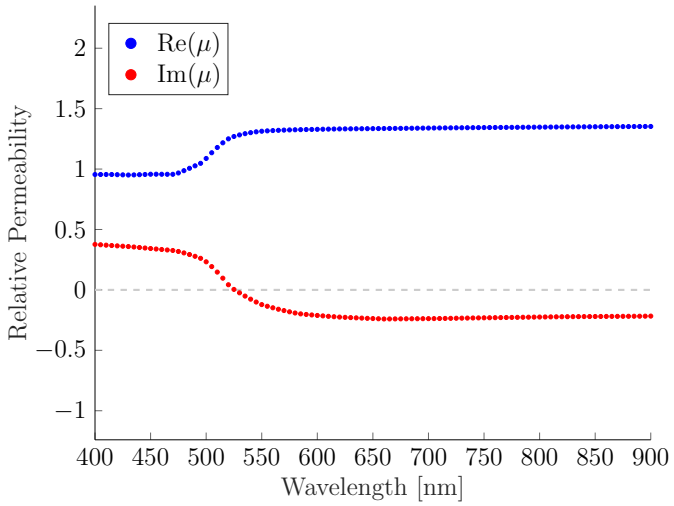

Figure 4.5: The relative permeability of a square array of gold cylinders with a radius of 12 nm and a period of 30 nm. The incident field is s-polarised. The relative permeability is calculated for an array of 10 rows thickness. The grey dashed line marks 0 on the y-axis for easier reading.

Figure 4.6 illustrates the real component of the refractive index of the metamaterial for different radii of the gold cylinders. When the cylinder radius is decreased, the period of the structure, i.e. the distance between the centres of the cylinders, is kept constant. This means that the gap between the cylinders increases as the radius decreases. All five curves are very close to each other, so the real part of the refractive index is mostly independent on the cylinder radius.

In Figure 4.7 the imaginary component of the refractive index of the metamaterial can be seen for different radii of the gold cylinders. Here it can be seen that the cylinder radius has a much larger impact on the imaginary part than it does on the real part, with larger cylinders resulting in a much larger imaginary part. As the metallic fraction of the metamaterial increases it is to be expected that the imaginary part also increases. Comparing this to Figure A.2 it can be seen that reducing the radius of the cylinders, while also reducing the period by the same factor, i.e.scaling the structure down, has the same effect of reducing the imaginary component of the refractive index, but to a much smaller degree.

Figure 4.8 shows a comparison between the effective refractive index for an array of either gold or silver cylinders. The two arrays are identical excepts for the material of the scatterers. The figure shows that the real part is mostly

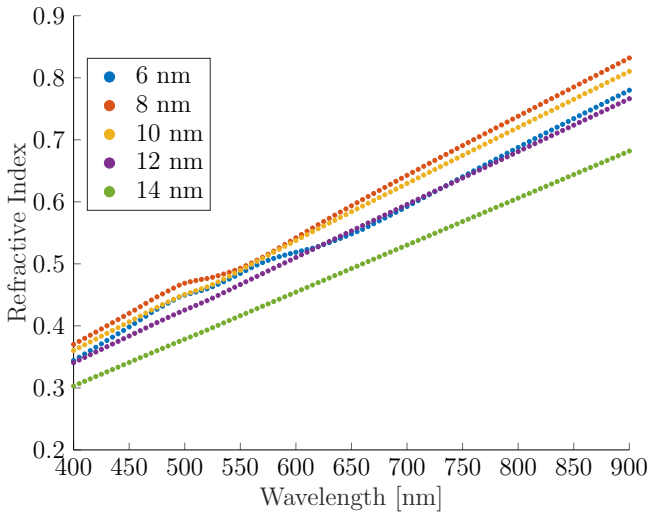

Figure 4.6: Comparison of the real component of the refractive index of a square array of gold cylinders of varying radius. The refractive index is calculated for a array of 10 rows thickness.

independent of the material, while the imaginary part follows the shape of the imaginary part for the bulk material. Silver cylinders gives a larger imaginary part than gold cylinders, which is to be expected, as this is also the case for the bulk materials. In Figure 4.9 and Figure 4.10 the real and imaginary parts of the refractive index can be seen for both a square array and a hexagonal array of gold cylinders. The hexagonal array is created by shifting every other row of cylinders half a period. This results in a hexagonal array which does not consist of equilateral hexagons, but it means that cylinders of the same size gives the same filling factor. From the figure is can be seen that changing the array pattern between square and hexagonal does not matter, as the curves are so close together that they are nearly impossible to distinguish from each other in both cases.

Figure 4.11 depicts the real part of the reflectance coefficient for a varying number of rows in the metamaterial. For the metamaterial to behave like a bulk material, the reflectance coefficient should be independent of the material thickness, as this is used to calculate the effective parameters. In the figure it can be seen that a single row of cylinders gives a significantly different reflectance coefficient, and while the curves get closer together as the number of rows increase. The curves showing the reflectance coefficient for 4 and 5 rows are difficult to

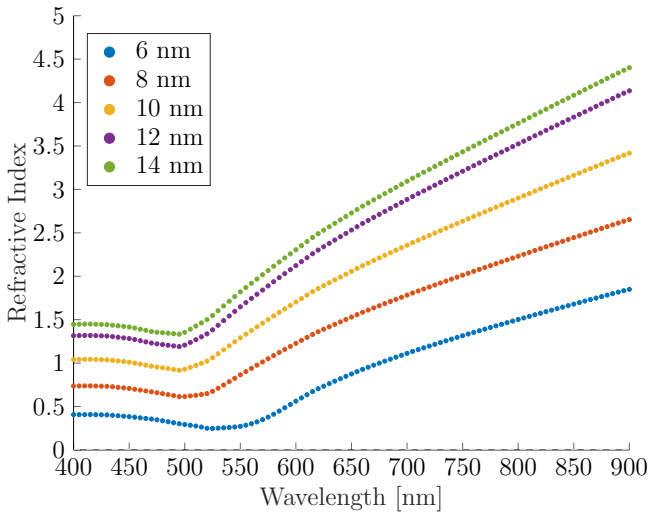

Figure 4.7: Comparison of the imaginary component of the refractive index of a square array of gold cylinders of varying radius, with a constant period of 30 nm. The refractive index is calculated for an array of 10 rows thickness.

distinguish for the majority of the spectrum, which means that by 4 rows, the matematerial will closely resemble a bulk material. In general it can be seen that the curves diverges more at longer wavelengths. In [13] it was shown that a similar matematerial, described in [16], using the same polarisation, started to behave as a bulk material around 3 rows, although that is for a much larger structure, and using a much longer wavelength.

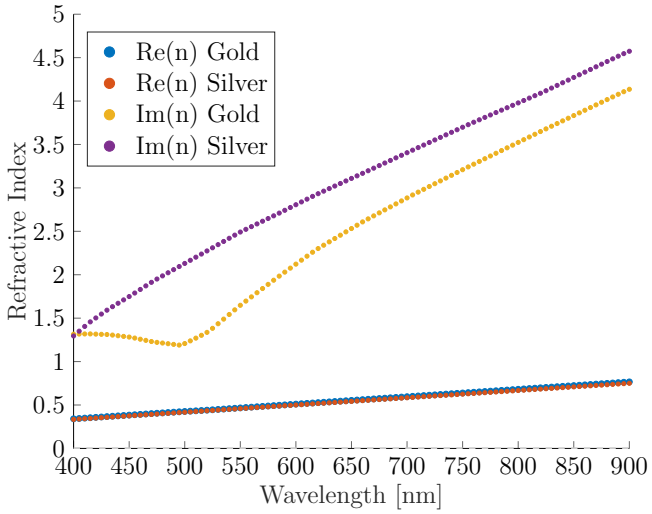

Figure 4.8: Comparison of the refractive index of a square array of either gold or silver cylinders of radius 12 nm and a period of 30 nm. The refractive index is calculated for an array of 10 rows thickness.

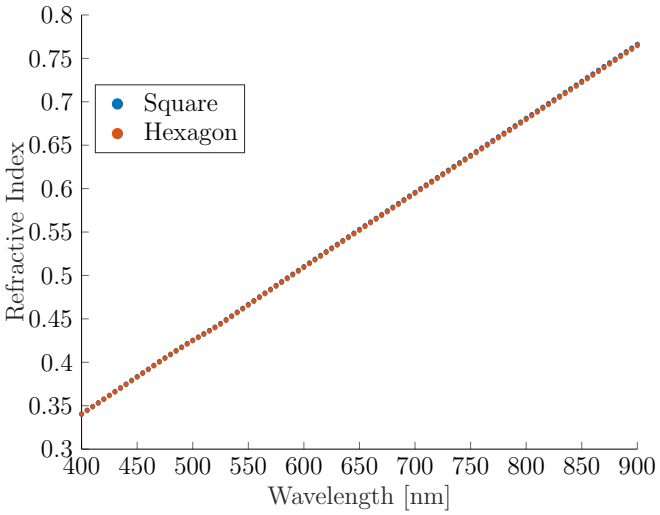

Figure 4.9: Comparison of the real component of the refractive index of either a square or hexagonal array of gold cylinders of radius 12 nm and a period of 30 nm. The refractive index is calculated for an array of 10 rows thickness.

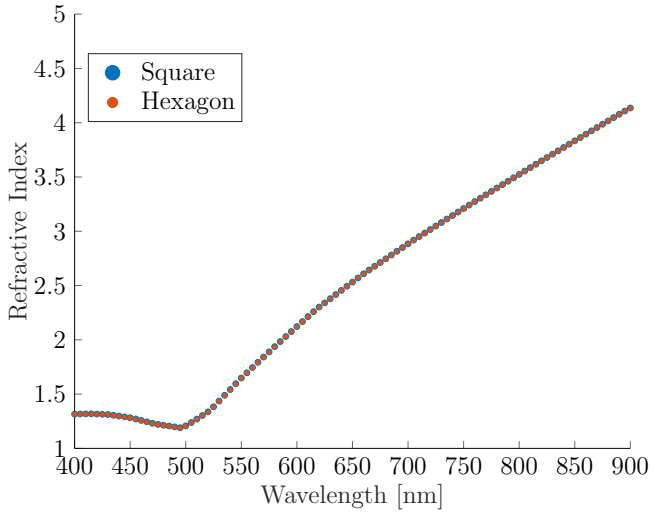

Figure 4.10: Comparison of the imaginary component of the refractive index of either a square or hexagonal array of gold cylinders of radius 12 nm and a period of 30 nm. The refractive index is calculated for an array of 10 rows thickness.

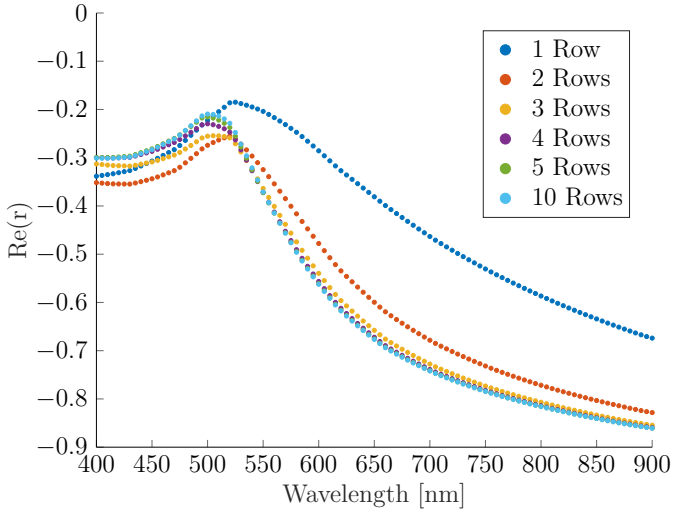

Figure 4.11: Comparison of the real part of the reflectance coefficient for a varying number of rows of a square array of gold cylinders of radius 12 nm and a period of 30 nm.

4.1.2 P-Polarisation

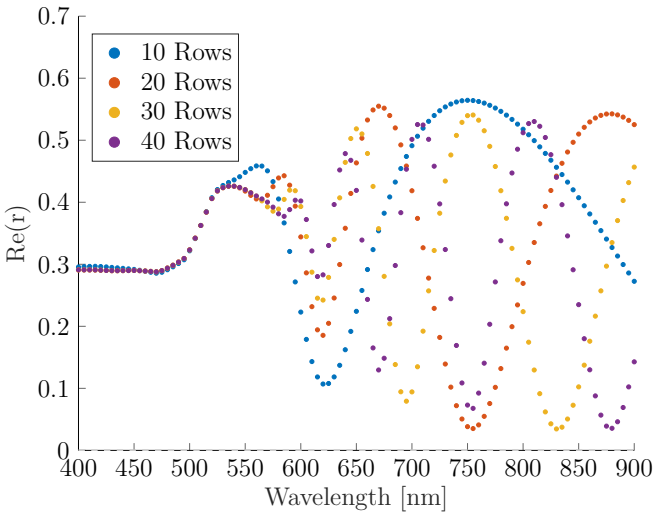

Figure 4.12: Comparison of the real part of the reflectance coefficient for a varying number of rows of a square array of gold cylinders of radius 12 nm and a period of 30 nm, for p-polarised light

Figure 4.12 shows the real part of the reflectance coefficient for a varying number of rows for the matematerial, for a p-polarised incident field. At short wavelengths the different thicknesses gives the same reflectance coefficient, as a bulk material should, but around 550 nm they diverge, which means that the metamaterial can not be treated as a bulk material at these wavelengths. As these thicknesses are much greater than the thickness at which the reflectance coefficient started to converge for the s-polarised case, it seems like the material will not converge at the longer wavelength end of the spectrum, even if the material was made thicker. As the reflectance coefficient is roughly the same for all thicknesses at short wavelengths, it might be possible to assign some effective parameters in this region. Comparing this figure to the refractive index of bulk gold, it can be seen that the reflectance coefficients starts to diverge after the imaginary refractive index starts to increase.

In Figure 4.13 and Figure 4.14 the absolute value of the reflectance coefficient can be seen for a varying number of rows of the metamaterial, for 12 nm and 8 nm respectively. While the reflectance varies highly with the number of rows, it can be seen that it is generally higher for larger cylinders, which is to be expected. For

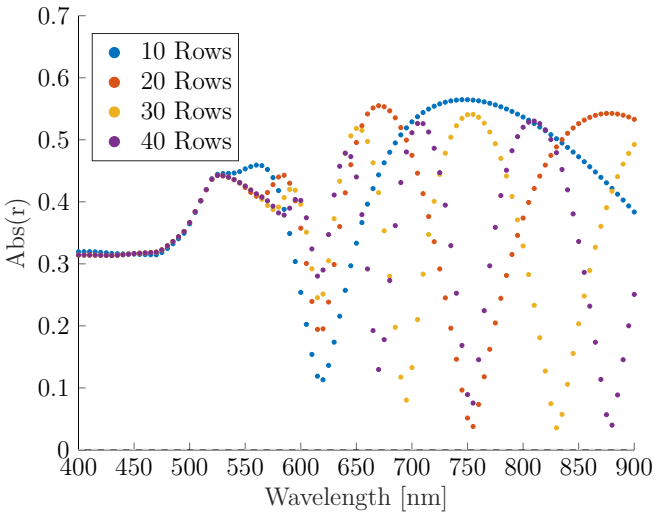

Figure 4.13: Comparison of the absolute value of the reflectance coefficient for a varying number of rows of a square array of gold cylinders of radius 12 nm and a period of 30 nm, for p-polarised light

the cylinders with a radius of 12 n, the reflectance coefficient seems to converge well at low wavelengths, but this is not the case for cylinders of 8 nm radius. In that case the only convergence point is around 760 nm, where all three curves shows no reflection. For an incident field to experience no reflection would imply the the refractive index is the same above and below the interface, if the Fresnel equations are considered. In this case it would imply that the effective refractive index is 1 for the metamaterial.

Figure 4.15 shows the imaginary component of the refractive index for an array of a varying number of gold cylinders. Comparing this to Figure 4.12, shows that the imaginary part of the refractive index is the same for different thicknesses in the region where the reflectance was also the same for different thicknesses. Beyond this region in the short wavelengths, the different thicknesses yields different results, which is to be expected, as a bulk material should give the same reflectance coefficient regardless of the thickness. Comparing the figure to Figure 4.1 it can be seen that the imaginary component is significantly lower for p-polarisation, which is consistent with Figure A.1. Comparing the figure to the imaginary component of the refractive index for thinner cylinders, as seen in Figure A.5, shows that the curves seem to follow the same shape, at least for

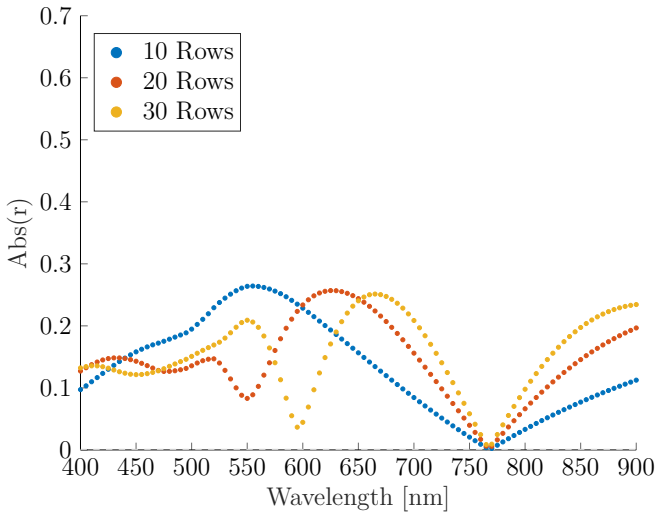

Figure 4.14: Comparison of the absolute of value the reflectance coefficient for a varying number of rows of a square array of gold cylinders of radius 8 nm and a period of 30 nm, for p-polarised light

short wavelength, although the values are much lower for the thinner cylinders. Both cylinder thickness seem to have a fairly well defined imaginary component of the refractive index for the short wavelengths, even though it is only the thicker cylinders that gives the same reflectance coefficient for different thicknesses in that region. Looking at the impedance for the different thicknesses of the cylinders and at different number of rows, Figure A.3, Figure A.4, Figure A.6 and Figure A.7, it can be seen that the impedance follows the same trend, with the curves following the same shape in the region where the reflectance coefficient is mostly independent of the thickness for the 12 nm cylinders, and crossing each other around the 760 nm point for the 8 nm cylinders.

The real part of the refractive index has not been calculated for the p-polarisation. This has been omitted because the correct branch has to be selected for the real part, and this selection is done by requiring that the different thickness yields the same result over a wider spectrum. This selection does not make sense when the different material thicknesses does not yield the same results for the reflectance coefficient.

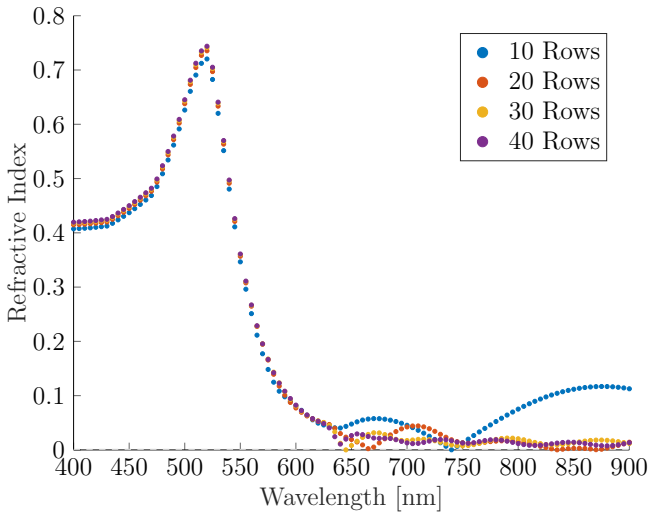

Figure 4.15: Comparison of the imaginary part of the refractive index for a varying number of rows of a square array of gold cylinders of radius 12 nm and a period of 30 nm, for p-polarised light

4.2 Scattering

When calculating the scattered field, the approach that used the wave equation for the total field was consistently yielding poor results, with a field that did not look as expected for a simple case of a single small cylinder. Additionally, this approach had a higher amount of noise, even with a high resolution of the structure. The figures in this section has therefore been calculated using the approach that considered the wave equation for the scattered field.

Figures 4.16 and 4.17 illustrate the total and scattered field for an array of gold cylinders, as well as the total and scattered field of a bulk material of the same size as the array, and using the effective parameters corresponding to that array. Assuming that a metamaterial can be considered a bulk material by assigning some effective parameters, the figures for the bulk material should resemble those for the array of scatterers. This also seems to be the case, although the bulk approximation shows a lower intensity towards the top and bottom, compared to the array. While it may look like the scattered field is weak between the cylinders, it is due to the markers for the cylinders, and the intensity is about the same as in the bulk approximation. In both cases the scattered field just about evens out the

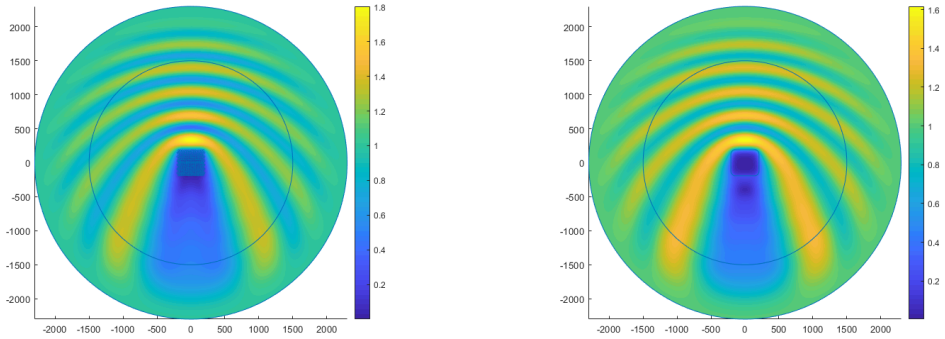

Figure 4.16: Left: The amplitude of the total electric field for a 13 by 13 array of gold cylinders. Right: The amplitude of the total electric field for a matematerial of the same size as the 13 by 13 array, using the effective parameters presented earlier.

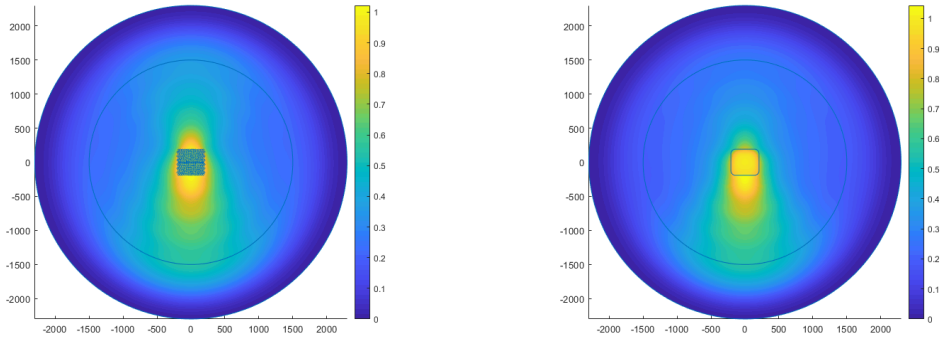

Figure 4.17: *The amplitude of the scattered electric field with the same setup as in Figure 4.16.*

incident field in the centre, resulting in a very weak field. This is to be expected, as it was seen above that the cylinder array will behave metallic.

In Figure A.8 the same figures are illustrated, but with an incident field with a wavelength of 500 nm. Once again the plots for the bulk approximation resembles the array fairly well. This is done to show that the bulk approximation is generally a good approximation across the spectrum, and not just accurate at a single wavelength by coincidence.

Comparing the scattered field from an array to the scattered field from randomly placed cylinders as seen in Figure A.9, it can be seen that the metamaterial still behaves like a metal.

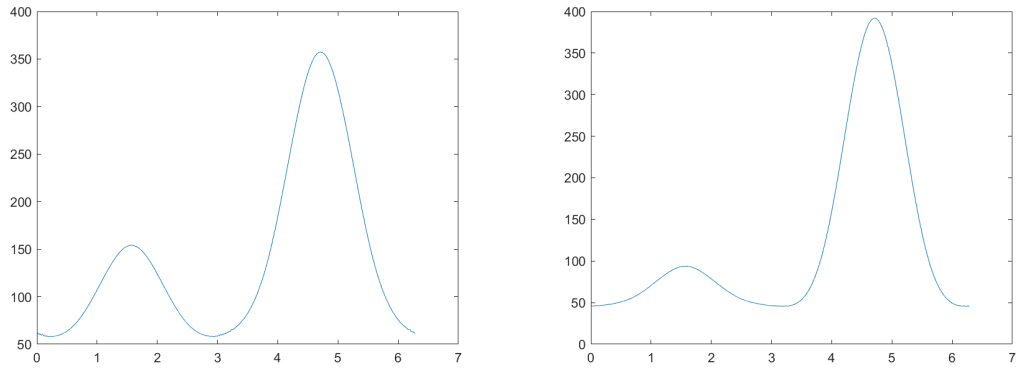

Figure 4.18: Left: The amplitude of the scattered field for a given angle, calculated for the cylinder array. Right: The amplitude of the scattered field for a given angle, calculated with the bulk approximation.

In Figure 4.19 the total and scattered field is depicted for an array of gold cylinders, with a p-polarised incident field. As the effective parameters have not been calculated for the p-polarisation, the array has not been approximated as a bulk material. Compared to Figure 4.16 and Figure 4.17, it can be seen that a greater portion of the light is reflected upwards, towards the incident field. The weak scattered field below the metamaterial means that the incident field mostly passes though the metamaterial, which is consistent with the results in the previous section. Comparing this to Figure A.9, where the cylinders are randomly distributed within a circle, it can be seen that the metamaterial behaves roughly the same when the cylinders are no longer placed in an array.

Figures 4.20 and 4.21 show the scattered and total fields of the metamaterial placed on a glass surface, calculated for an array of gold cylinders, and a bulk material with the corresponding effective parameters. The metamaterial is placed so that half of it is above the surface and half of it is below. The refractive index used for the glass is $n_{glass} = 1.5$, and the surface is marked by the horizontal blue line in all four figures. The centre of the scattered field for the array of cylinders looks darker than it is due to the markers for the cylinders. Comparing this plot to the scattered fields without the surface, Figures 4.16 and 4.17, it can be seen that more light is scattered downwards when the surface is present. The bulk material approximation seems to work well, even when the setup is made more

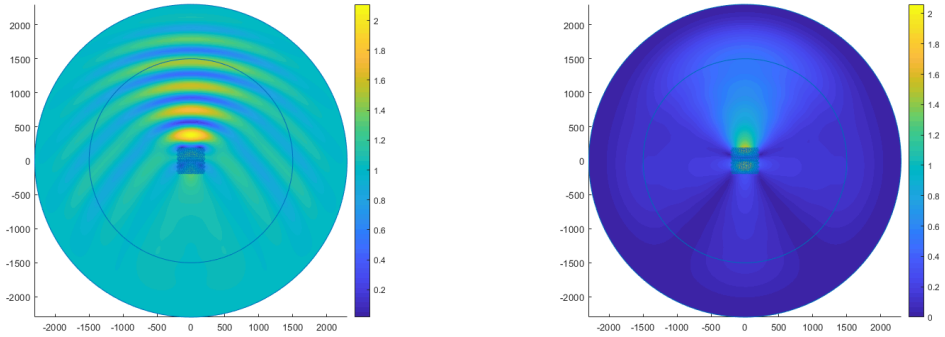

Figure 4.19: Left: The amplitude of the total magnetic field for a 13 by 13 array of gold cylinders. Right: The amplitude of the scattered electric field by a the same array of gold cylinders. The plots are made with an incident magnetic field which is a plane wave and parallel to the cylinders (p-polarised) and has a wavelength of 700 nm. The incident magnetic field has an amplitude of 1 and comes in from the top of the figures. The outer blue circle marks the beginning of the PML.

complicated. In Figures 4.22 and 4.23 the same setup can be seen, but with an incident field rotated 45 degrees counterclockwise.

In Figure 4.24 and Figure 4.25 the scattering cross section at different angles for the incident field is depicted. This is calculated for a free metamaterial as well as a metamaterial submerged halfway into a glass surface, as depicted in Figures 4.20 and 4.21, and it has been calculated using both an array of gold cylinders and as a bulk approximation. The plot is made with a s-polarised incident field. For the free metamaterial the incident field changes from an angle of 0 relative to the y-axis, which corresponds to normal incidence on the surface of the metamaterial, to an angle of 45 degrees, which corresponds to the direction of the light pointing straight at the corner of the metamaterial. Changing the angle further would not give any new results because of the symmetry in this setup. From the figure it can be seen that the scattering cross section decreases as the angle increases, although not by much. The same hold true for the case with the surface, but to a much larger degree. Note that the scattering cross section has been plotted for a larger variation in the angle, as this case only has symmetry around the y-axis, due to the surface. The greatest angle for which the scattering cross section has been calculated corresponds to an angle of 22.5 degrees relative to the glass surface.

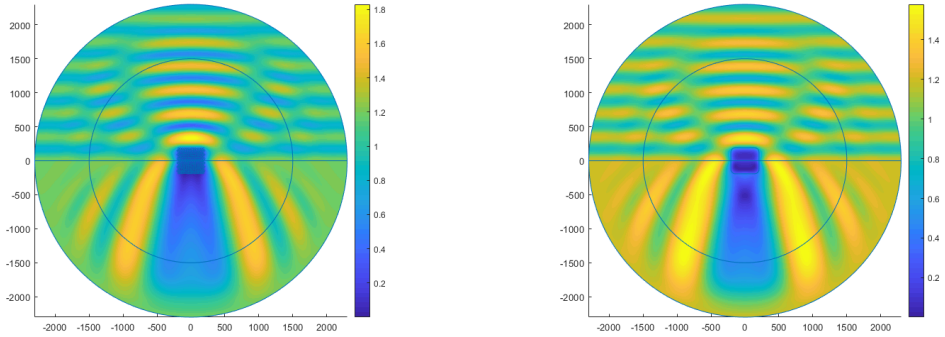

Figure 4.20: Left: The amplitude of the total electric field for a 13 by 13 array of gold cylinders, submerged halfway into a glass surface. Right: The amplitude of the total electric field for a matematerial of the same size as the 13 by 13 array, using the effective parameters.

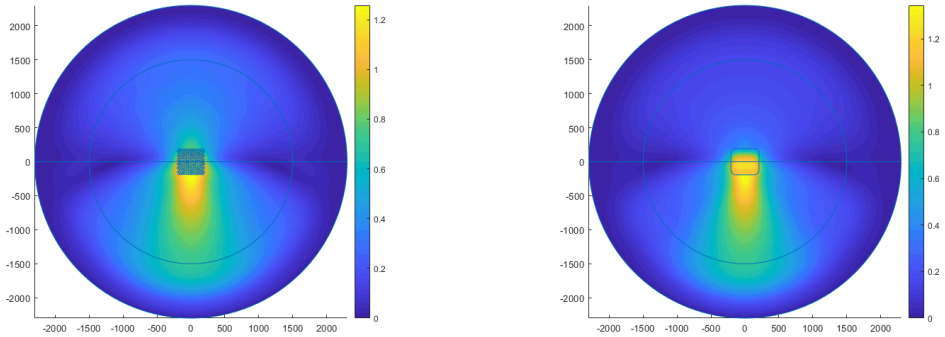

Figure 4.21: The amplitude of the scattered electric field with the same setup as in Figure 4.20.

For both cases the bulk approximation gives a lower scattering cross section.

Figures 4.16, 4.17, 4.20, 4.21 4.22 and 4.23, are made with an incident electric field which is a plane wave and parallel to the cylinders (s-polarised) and has a wavelength of 700 nm. The incident electric field has an amplitude of 1 and comes in from the top of the figures. The blue circle marks the beginning of the PML. In the figures where it is present, a horizontal blue line marks the glass surface.

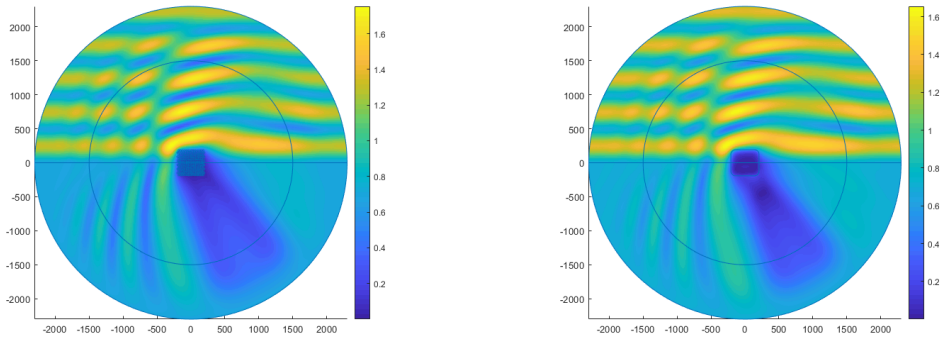

Figure 4.22: Left: The amplitude of the total electric field for a 13 by 13 array of gold cylinders, submerged halfway into a glass surface. Right: The amplitude of the total electric field for a matematerial of the same size as the 13 by 13 array, using the effective parameters presented earlier. The incident electric field comes in from the top left of the figures, at an angle of 45 degrees relative to the surface.

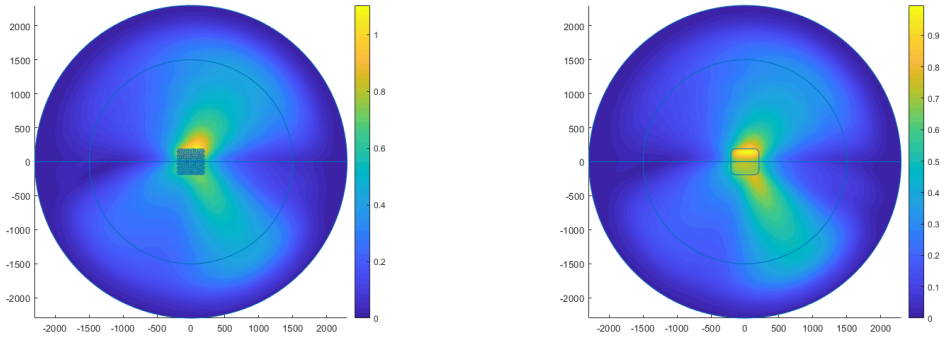

Figure 4.23: The amplitude of the scattered electric field with the same setup as in Figure 4.22.

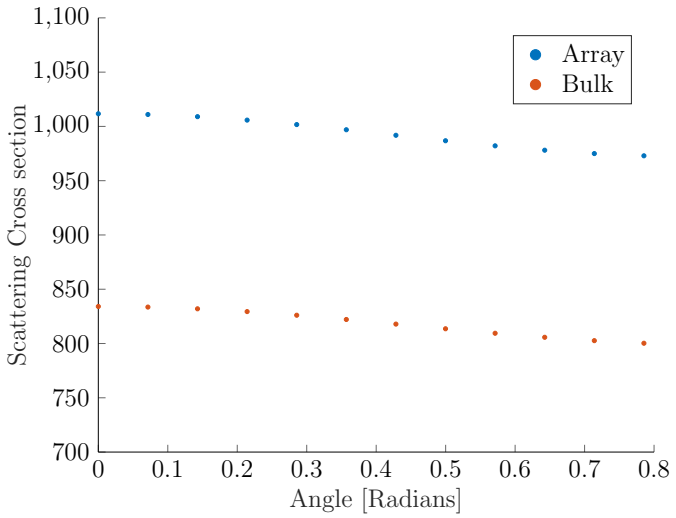

Figure 4.24: The scattering cross section at different angles, for a 13 by 13 array of gold cylinders of radius 12 nm and period 30 nm, as well as a bulk material of same size as the array, using the corresponding effective parameters. 0 degrees corresponds to an incident field normal to the matematerial surface. The incident field is s-polarised, with an amplitude of 1.

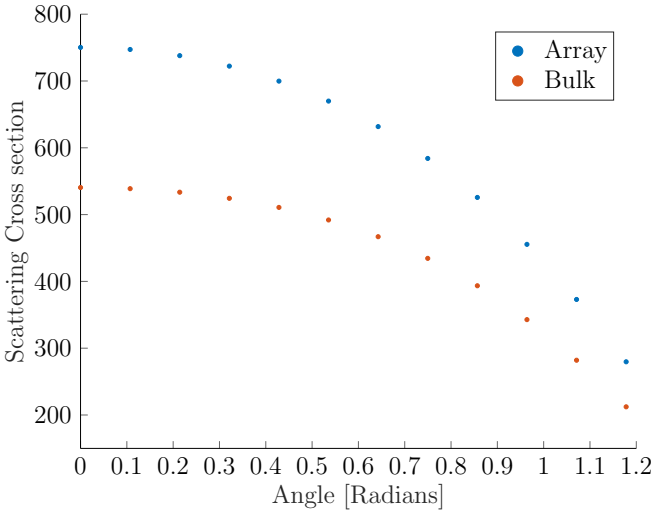

Figure 4.25: The scattering cross section at different angles, for a 13 by 13 array of gold cylinders of radius 12 nm and period 30 nm, half submerged into a glass surface with refractive index 1.5, as well as a bulk material of same size as the array, using the corresponding effective parameters. 0 degrees corresponds to an incident field normal to the matematerial surface, as well as the glass surface. The incident field is s-polarised, with an amplitude of 1.

4.3 The Numerical Methods

The program used to calculate the reflectance and transmittance coefficients seems to be fairly unaffected by noise in the calculations for the reflectance and transmittance coefficient. In Figure A.10 it can be seen that the distance above the first unit cell, for which the reflectance coefficient is calculated, has a very little impact of the reflectance coefficient , and it has converged reasonably well to some value by 50 nm. Note that this was measured for a wavelength of 700 nm, and a higher wavelength might show that a larger spacing is required, but this should not change a lot for 900 nm, which is the longest wavelength considered in this report. In Figure A.11 it can be seen that a large maximum length for the triangle sides still gives a fairly accurate measurement for the reflectance coefficient. While the reflectance coefficient seems to converge continuously for the spacing, the reflectance coefficient as a function of hmax is discrete. This might be explained as the number of triangles in a single cylinder remaining constant for a while when hmax is large, and the jumps could occur at the points where the number of triangles changes. This would not be as noticeable for low values of hmax, where the number of triangles changes with every change in the value of hmax. The fast convergence with respect to spacing and triangle side length means that the program takes a very short time to run, while still giving acceptable results. This is important, as the program often has to be run a large amount of times to give the reflectance and transmittance coefficients for a wide spectrum with a good resolution, and for different material thicknesses, to give a good approximation for the effective parameters.

The program used for calculating the scattered field takes a significantly higher amount of triangles to achieve acceptable results, as can be seen in Figure A.12, and so a compromise between time and accuracy has to be made in this case. This is to be expected, as both the area and number of cylinders will typically be much larger in this program. The calculations for the scattered field requires the normal vector to the surface of the scatterers, which means that these needs a high resolution. This also means that a good approximation for the effective parameters of the metamaterial will greatly reduce the run time of program, as the surface area of the scatterer will often be reduced significantly by considering the metamaterial

as a bulk material, and the surface will often be smoother, meaning that the resolution required to get acceptable normal vectors will be lower. Comparing Figure A.12 to Figure A.13 shows that the variation in the scattering cross section due to a change in hmax, is smaller with the bulk approximation.

5

Conclusion

Contents

3.1 Creation of Structure 43

3.2 Mesh Generation 44

3.3 Selection of Zones 46

3.4 Calculation of the Scattered Field 47

When calculating the effective parameters for a given metamaterial, it was found the the simpler approaches, such as taking the weighted average, was insufficient, and the approach which used the relations between the reflectance and transmittance coefficient and the refractive index and impedance yielded the best results.

Assigning effective parameters to a metamaterial consisting of metal cylinders went reasonably well when the incident field was s-polarised and the metamaterial was found to behave roughly like a metal. The effective refractive index followed the same shape as the corresponding bulk refractive index for the metal of the cylinders, but the actual values for the effective refractive index could be altered by changing the parameters of the structure, particularly the imaginary part. Unlike its constituent part, e.g. gold and air, the metamaterial was found to have a permeability different from 1. For p-polarised light, the effective parameters was found to be dependent on the thickness of the metamaterial, which means that it cannot be approximated as a bulk material. It could be seen that for some regions of the spectrum the reflectance coefficient was independent of the thickness of the metamaterial, meaning that the effective parameters could be approximated to some extent in these regions. However, due to the way the real part of the effective refractive index was calculated, it would be difficult to get a good approximation for this, even in those region. Another problem was that these regions were highly dependent of the parameters of the structure, e.g. for a cylinder radius of 12 nm the region was the short wavelength end of the spectrum, but for a cylinder radius of 8 nm it was only in a very small area around 760 nm. This means that for the structure we have considered, the metamaterial cannot be approximated as a bulk material for a p-polarised incident field. The metamaterial was found to behave much more like a dielectric when the incident field was p-polarised.

For the scattered field it was found that the metamaterial could be approximated reasonably well as a bulk material, although it was found the the scattered field was generally weaker with the bulk approximation. When the metamaterial was placed on a surface with a higher refractive index, in this case glass, the amplitude of the scattered field was stronger in under the surface, than it would have been without the surface. For both a free square metamaterial and a square meta-

material on a surface it was found that the scattering cross section was greatest for an incident field normal to the metamaterial and surface, and that the scattering cross section decreases faster with a change in the angle for the case with a surface. Concerning the two methods for calculating the scattered field, the method which used the wave equation for the scattered field was found to be better, as the method which used the wave equation for the total field had a large degree of noise, even at very high resolutions.

Future Works

As mentioned in Section 2.2, the shape functions used were linear polynomials. As such, the triangular elements in the mesh needed only 3 nodes. Another possibility would be to use quadratic polynomials instead. As a result, 36 different polynomials would have to be calculated, as there would now be 6 nodes. It would be interesting to examine how much of a difference this change would make. Depending on how much precision is gained, it would be possible to lower the resolution of the mesh which, in turn, would reduce computation time. Luckily, computation time was not a large factor in this project, as the developed script had been optimised.

Additional optimisation of the script could be done. As Matlab by default only uses one CPU core, as long as each iteration of a for-loop is independent of the others, one could use the 'Parallel Computing Toolbox'. This toolbox includes an alteration of the default for-loop, called *parfor*, and allows Matlab to assign the iterations of the for-loop to all available cores.

In this project, the examination of metamaterials were chosen to be in two dimensions. From a theoretical point of view, expanding this into three dimensions could be done with the same principles. It would, however, render all the developed code useless, and one would have to develop a script from scratch, as little common ground can be found.

Another possible expansion would be to examine larger structures using larger wavelengths. Larger structures are more easily produced, which would make experimental corroboration a lot more likely. A number of articles already exist

which examine structures in the millimetre domain using wavelengths in the microwave spectrum. Unfortunately, the available date on the refractive indices of gold and silver as a function of wavelength were limited to wavelengths between 200 and 1900 nm. The density of available data points decreased with an increase in wavelength, and since interpolation has been used, wavelengths beyond 900 nm have not been considered, although a Drude model for the permittivity could be used at long wavelength.

References

[1] N. Schlömer *et al.*, [Accessed June 6, 2018]. [Online]. Available: https://se.mathworks.com/matlabcentral/fileexchange/22022-matlab2tikz-matlab2tikz

[2] R. S. Cruz and P. Tomás, [Accessed June 6, 2018]. [Online]. Available: https://www.overleaf.com/latex/templates/ist-ul-msc-thesis/wrhbmbvzpttw

[3] [Accessed June 6, 2018]. [Online]. Available: https://www.beautifulchemistry.net/nanoparticles/

[4] D. R. Smith, W. J. Padilla, D. C. Vier, S. C. Nemat-Nasser, and S. Schultz, "Composite medium with simultaneously negative permeability and permittivity," *Physical Review Letters*, vol. 84, no. 18, 5 2000.

[5] B. D. J. and F. I. C., "An investigation of the origin of the colour of the lycurgus cup by analytical transmission electron microscopy," *Archaeometry*, vol. 32, no. 1, pp. 33–45. [Online]. Available: https://onlinelibrary.wiley.com/doi/abs/10.1111/j.1475-4754.1990.tb01079.x

[6] L. Novotny and B. Hecht, *Principles of Nano-Optics*, ser. Principles of Nano-optics. Cambridge University Press, 2012. [Online]. Available: https://books.google.dk/books?id=FUAAxtxvGI4C

[7] A. Polycarpou, *Introduction to the Finite Element Method in Electromagnetics*, ser. Online access: IEEE (Institute of Electrical and Electronics Engineers) IEEE Morgan & Claypool Synthesis eBooks Library. Morgan & Claypool Publishers, 2006. [Online]. Available: https://books.google.dk/books?id=BROAaKKsMjIC

[8] E. Kreyszig, *Advanced Engineering Mathematics*. John Wiley & Sons, 2010. [Online]. Available: https://books.google.dk/books?id=UnN8DpXI74EC

[9] T. Søndergaard, "Finite element method exercise 1, calculating reflectance and transmittance from a metal array." 2018.

[10] ——, "Finite element method exercise 2, calculating the scattering from a dielectric scatterer." 2018.

[11] E. Hecht, *Optics*, ser. Pearson education. Addison-Wesley, 2002. [Online]. Available: https://books.google.dk/books?id=T3ofAQAAMAAJ

[12] W. Cai and V. Shalaev, *Optical Metamaterials: Fundamentals and Applications*. Springer New York, 2009. [Online]. Available: https://books.google.dk/books?id=q8gDF2pbKXsC

[13] D. R. Smith, S. Schultz, P. Markoš, and C. M. Soukoulis, "Determination of effective permittivity and permeability of metamaterials from reflection and transmission coefficients," *Phys. Rev. B*, vol. 65, p. 195104, Apr 2002. [Online]. Available: https://link.aps.org/doi/10.1103/PhysRevB.65.195104

[14] X. Chen, T. M. Grzegorczyk, B.-I. Wu, J. Pacheco, and J. A. Kong, "Robust method to retrieve the constitutive effective parameters of metamaterials." *Physical review. E, Statistical, nonlinear, and soft matter physics*, vol. 70 1 Pt 2, p. 016608, 2004.

[15] V. Markel, "Can the imaginary part of permeability be negative?" *The American Physical Society, http://dx.doi.org/10.1103/PhysRevE.78.026608*, 2008.

[16] P. Marko and C. M. Soukoulis, "Transmission studies of left-handed materials," 2001.

A

Additional Results

A.1 Effective Parameters

Figure A.1: Left: The amplitude of the electric field throughout an array of gold cylinders with a radius of 12 nm and period of 30 nm. Right: The amplitude of the magnetic field throughout the same array. In both cases the incident field is coming in from the top and has an amplitude of 1. The circles marks the gold cylinders.

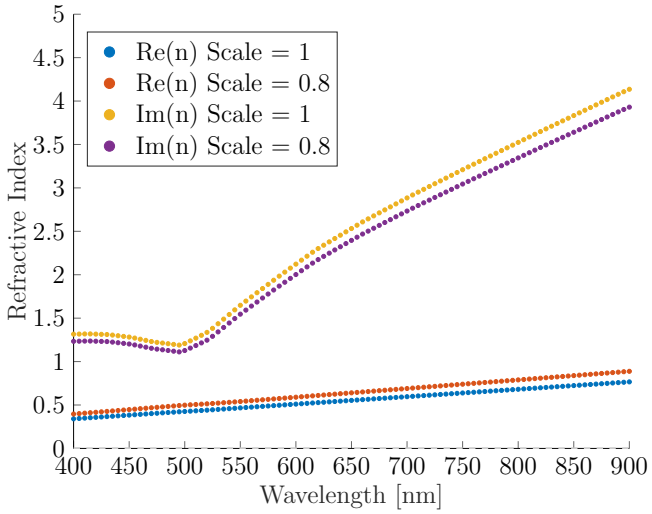

Figure A.2: Comparison of the refractive index, for a array of gold cylinders with a radius of 12 nm and a period of 30 nm, and the refractive index for the same array scaled by a factor of 0.8.

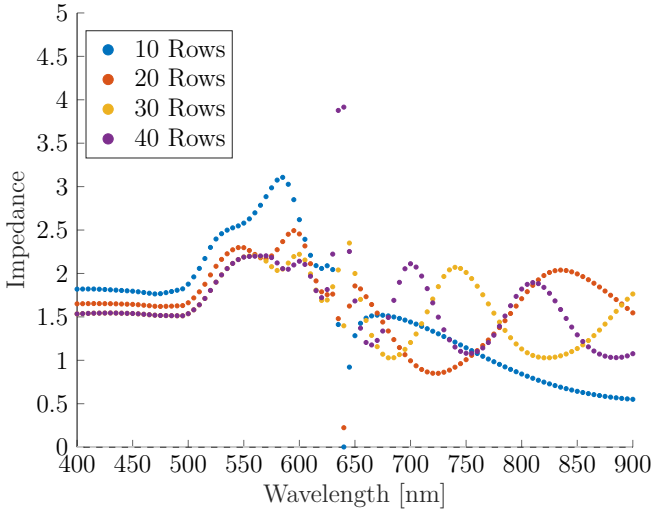

Figure A.3: Comparison of the real part of the impedance for a varying number of rows of a square array of gold cylinders of radius 12 nm and a period of 30 nm, for p-polarised light

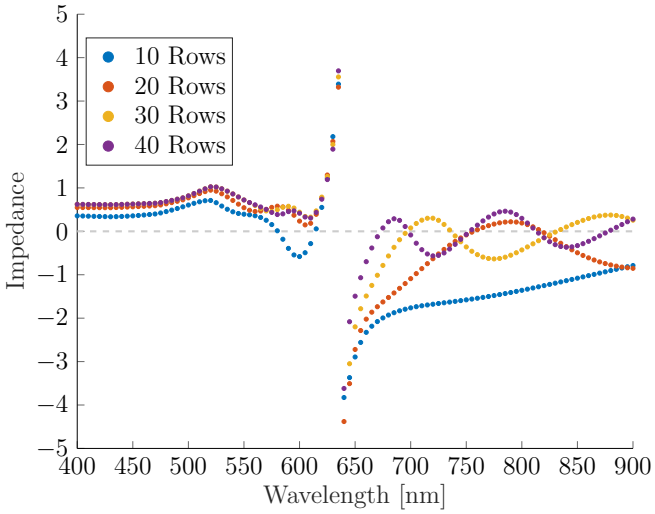

Figure A.4: Comparison of the imaginary part of the impedance for a varying number of rows of a square array of gold cylinders of radius 12 nm and a period of 30 nm, for p-polarised light

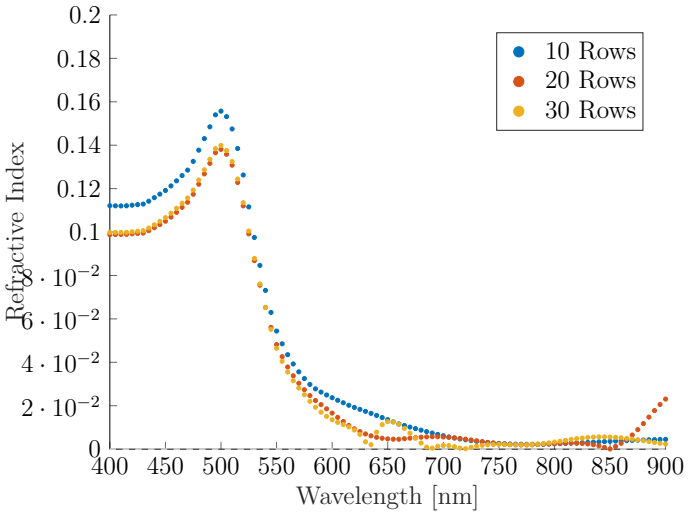

Figure A.5: Comparison of the imaginary part of the refractive index for a varying number of rows of a square array of gold cylinders of radius 8 nm and a period of 30 nm, for p-polarised light

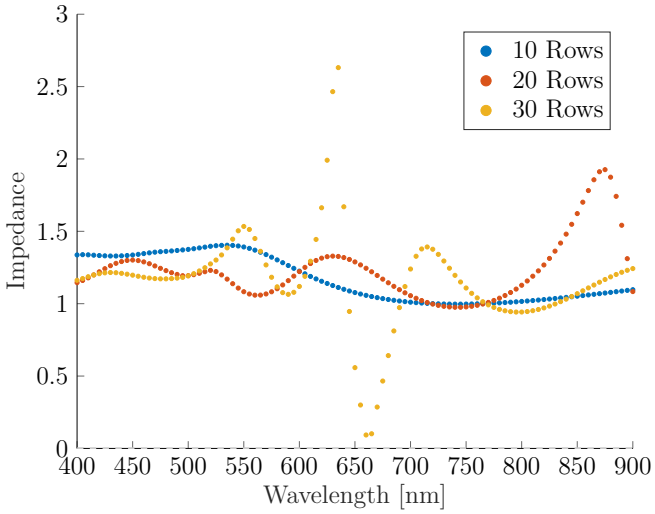

Figure A.6: Comparison of the real part of the impedance for a varying number of rows of a square array of gold cylinders of radius 8 nm and a period of 30 nm, for p-polarised light

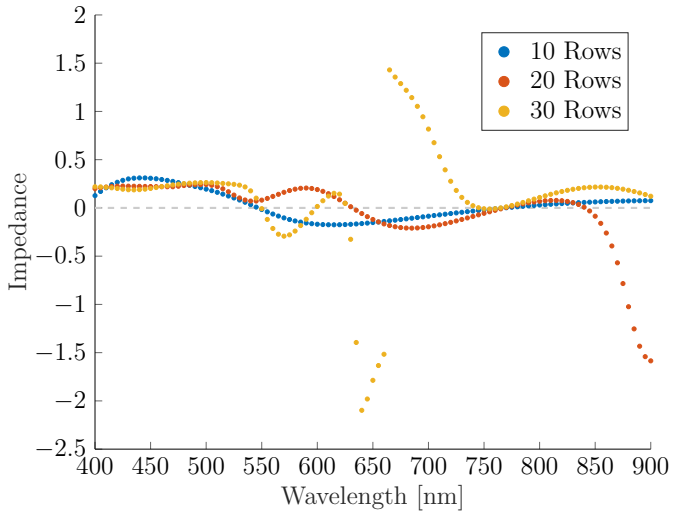

Figure A.7: Comparison of the imaginary part of the impedance for a varying number of rows of a square array of gold cylinders of radius 8 nm and a period of 30 nm, for p-polarised light

A.2 Scattering

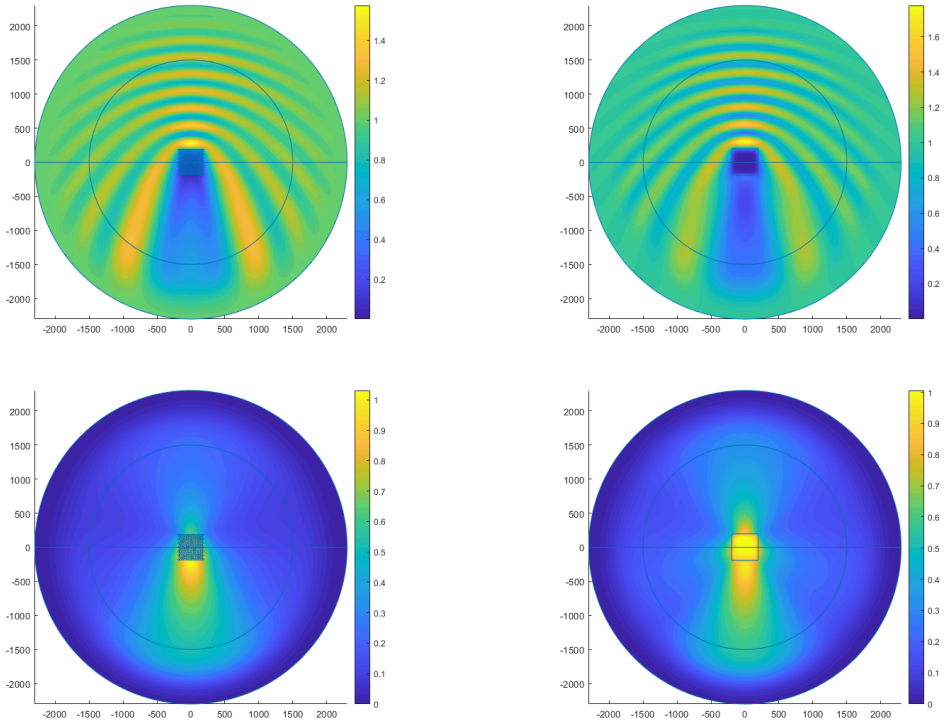

Figure A.8: Top left: The amplitude of the total electric field for a 13 by 13 array of gold cylinders. Top right: The amplitude of the total electric field for a matematerial of the same size as the 13 by 13 array, using the effective parameters presented earlier. Bottom left: The amplitude of the scattered electric field by a the same array of gold cylinders. Bottom right: The amplitude of the scattered field by the same metamaterial. All the plots are made with an incident electric field with is a plane wave and parallel to the cylinders (s-polarised) and has a wavelength of 500 nm. The incident electric field has an amplitude of 1 and comes in from the top of the figures.

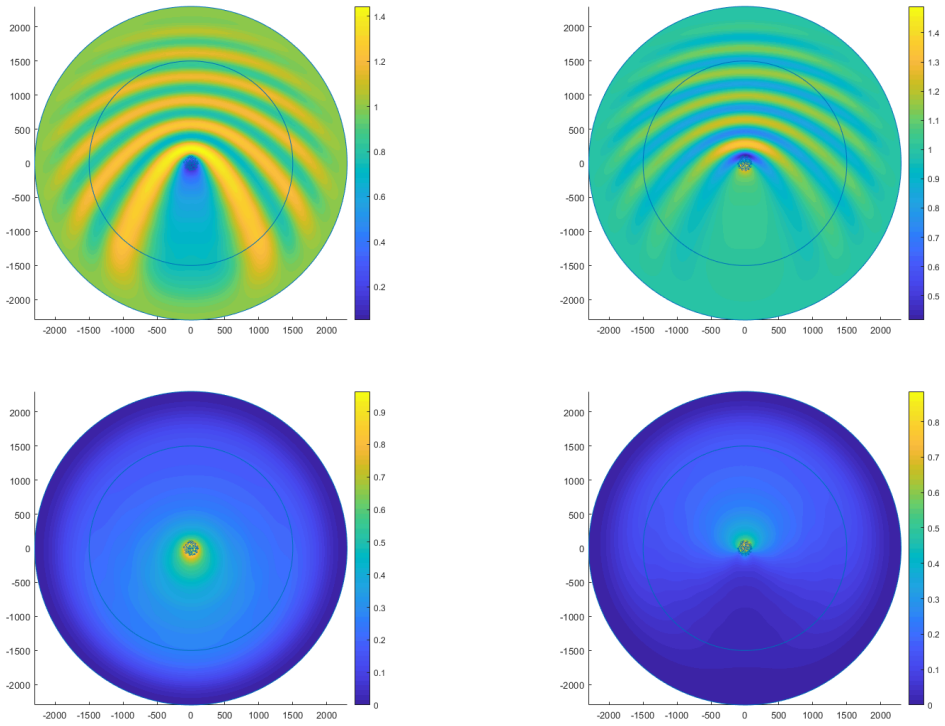

Figure A.9: Top left: The amplitude of the total electric field for randomly placed gold cylinders. Top right: The amplitude of the total magnetic field for randomly placed gold cylinders. Bottom left: The amplitude of the scattered electric field by randomly placed gold cylinders. Bottom right: The amplitude of the scattered magnetic field by randomly placed cylinders. All the plots are made with an incident electric or magnetic field which is a plane wave and parallel to the cylinders and has a wavelength of 700 nm, and an amplitude of 1. The metamaterial is 100 gold cylinders of radius 12, placed randomly in a circle with a radius of 100 nm. The cylinders are added till the circle is filled, with no cylinder being closer than 4 nm to another.

A.3 Convergence

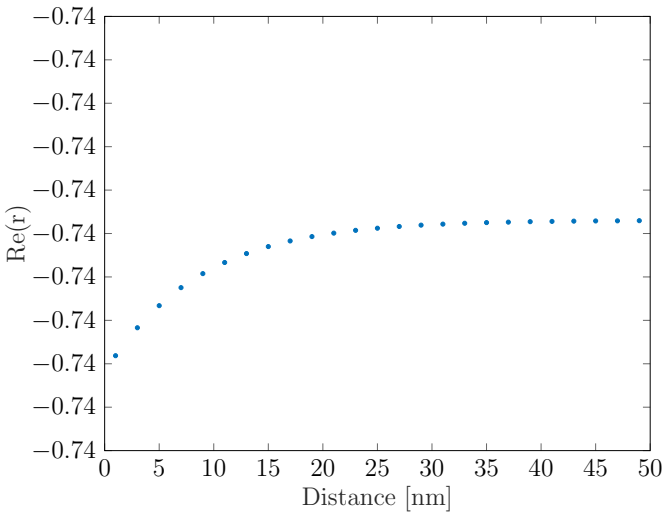

Figure A.10: The real part of the reflectance coefficients for a square array of gold cylinders with a radius of 12 nm and a period of 30 nm, measured at different distances above the start of the first unit square, which is defined as the half a period above the centre of the first cylinder. The measurement was made with 15 rows of gold cylinders. The y-axis goes from -0.74 to -0.745.

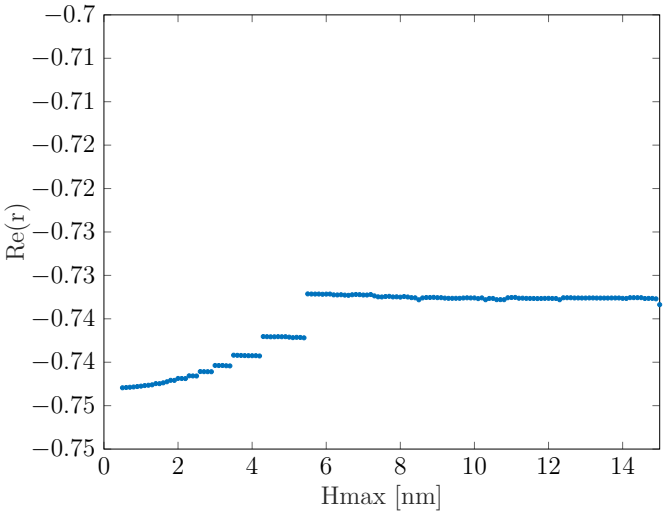

Figure A.11: The real part of the reflectance coefficients for a square array of gold cylinders with a radius of 12 nm and a period of 30 nm, calculated for meshes with different values for hmax, the largest allowed side length for a triangle. The measurement was made with 15 rows of gold cylinders.

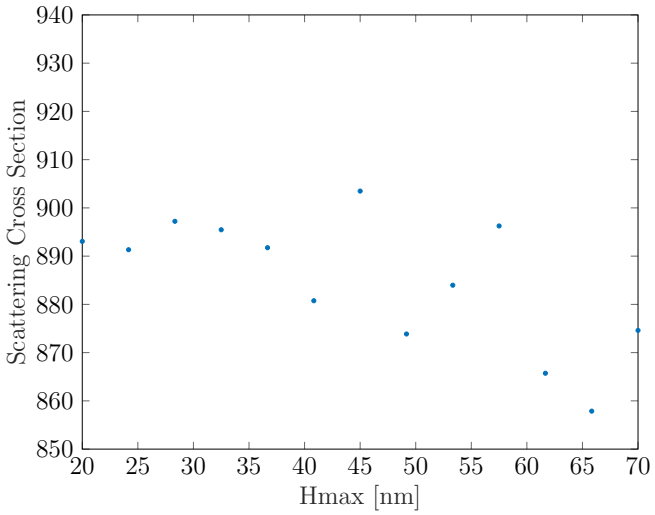

Figure A.12: The scattering cross section for an 13 by 13 array of gold cylinders, calculated with a mesh created for different values of hmax, the largest allowed side length for a triangle. The cylinders had a radius of 12 nm and a period of 30 nm. The mesh inside the cylinders were "refined" twice, meaning that each triangle were halved twice. The initial minimal triangle side length is one quarter of the hmax.

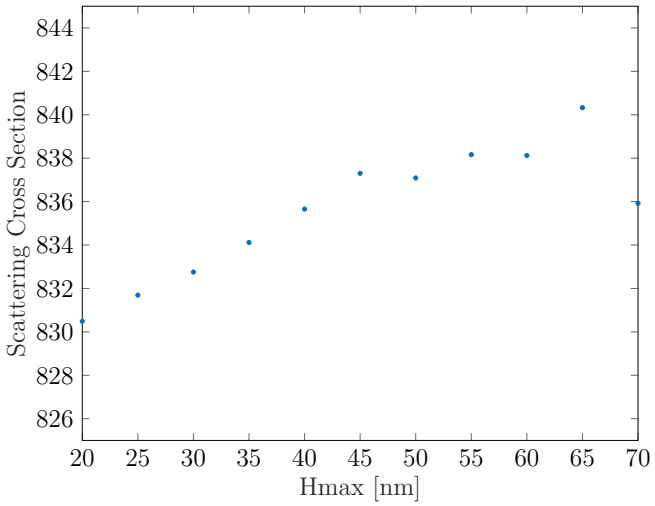

Figure A.13: The scattering cross section for an 390 nm by 390 nm bulk material, using the appropriate effective parameters, calculated with a mesh created for different values of hmax, the largest allowed side length for a triangle. The cylinders had a radius of 12 nm and a period of 30 nm. The mesh inside the cylinders were "refined" twice, meaning that each triangle were halved twice. The initial minimal triangle side length is one quarter of the hmax.

B

Matlab Code

B.1 A Matrix and M Insertion

```
%% Calculations.

for i = 1:n_tri

    zone = t(end,i);

    % Choose parameters depending on which zone the current
    % triangle resides in.
    if any(zone == obj_zone.upper)

        diel_const = di_const_env;
        mag_const = mag_const_env;

    elseif any(zone == obj_zone.lower)
```

```
        diel_const = di_const_surf;
        mag_const = mag_const_surf;

    elseif any(zone == obj_zone.scat)

        diel_const = di_const_scat;
        mag_const = mag_const_scat;

    end

    ref_ind = sqrt(diel_const);

    xy_val = p(:,t(1:3,i));

    x1 = xy_val(1,1);
    x2 = xy_val(1,2);
    x3 = xy_val(1,3);
    y1 = xy_val(2,1);
    y2 = xy_val(2,2);
    y3 = xy_val(2,3);

    area_tri_i = abs((((x2 - x1) * (y3 - y1))...
                -      ((y2 - y1) * (x3 - x1))))/2;

    du_dx =  (y3 - y1)/((y3 - y1) * (x2 - x1)...
                      - (y2 - y1) * (x3 - x1));
    dv_dx =  (y2 - y1)/((y2 - y1) * (x3 - x1)...
                      - (y3 - y1) * (x2 - x1));
    du_dy = -(x3 - x1)/((y3 - y1) * (x2 - x1)...
```

```
                    - (y2 - y1) * (x3 - x1));
dv_dy = -(x2 - x1)/((y2 - y1) * (x3 - x1)...
                    - (y3 - y1) * (x2 - x1));


d11 = (-1*du_dx - 1*dv_dx) * (-1*du_dx - 1*dv_dx)...
    + (-1*du_dy - 1*dv_dy) * (-1*du_dy - 1*dv_dy);
d12 = (-1*du_dx - 1*dv_dx) * (+1*du_dx + 0*dv_dx)...
    + (-1*du_dy - 1*dv_dy) * (+1*du_dy + 0*dv_dy);
d13 = (-1*du_dx - 1*dv_dx) * (+0*du_dx + 1*dv_dx)...
    + (-1*du_dy - 1*dv_dy) * (+0*du_dy + 1*dv_dy);
d21 = (+1*du_dx + 0*dv_dx) * (-1*du_dx - 1*dv_dx)...
    + (+1*du_dy + 0*dv_dy) * (-1*du_dy - 1*dv_dy);
d22 = (+1*du_dx + 0*dv_dx) * (+1*du_dx + 0*dv_dx)...
    + (+1*du_dy + 0*dv_dy) * (+1*du_dy + 0*dv_dy);
d23 = (+1*du_dx + 0*dv_dx) * (+0*du_dx + 1*dv_dx)...
    + (+1*du_dy + 0*dv_dy) * (+0*du_dy + 1*dv_dy);
d31 = (+0*du_dx + 1*dv_dx) * (-1*du_dx - 1*dv_dx)...
    + (+0*du_dy + 1*dv_dy) * (-1*du_dy - 1*dv_dy);
d32 = (+0*du_dx + 1*dv_dx) * (+1*du_dx + 0*dv_dx)...
    + (+0*du_dy + 1*dv_dy) * (+1*du_dy + 0*dv_dy);
d33 = (+0*du_dx + 1*dv_dx) * (+0*du_dx + 1*dv_dx)...
    + (+0*du_dy + 1*dv_dy) * (+0*du_dy + 1*dv_dy);


% x and y coordinates of middle of triangle.
x_mid_tri = ((max(xy_val(1,:)) - min(xy_val(1,:)))/2)...
          +   min(xy_val(1,:));
y_mid_tri = ((max(xy_val(2,:)) - min(xy_val(2,:)))/2)...
          +   min(xy_val(2,:));
```

```
fun_ang = cos(theta) * x_mid_tri + sin(theta) * y_mid_tri;

E0 = exp(1i * k0 * ref_ind * fun_ang);

r_0 = r_env;

sigma_0 = 6*log(10)/(2*pi/lambda*r_PML.^3);

% If the current triangle resides in the PML zone.
if any(zone == obj_zone.PML)

    r_mid_tri = sqrt(x_mid_tri.^2 + y_mid_tri.^2);

    sigma = sigma_0/diel_const * (r_mid_tri - r_0).^2;

else

    sigma = 0;

end

A = (area_tri_i...
  * [d11 d12 d13 ; d21 d22 d23 ; d31 d32 d33])...
 ./ (1 + 1i * sigma).^2;

switch polarisation

    case 'p'
```

```
            Mk = k0^2 * B * area_tri_i * mag_const...
                - A/diel_const;

        case 's'

            Mk = k0^2 * B * area_tri_i * diel_const...
                - A/mag_const;

    end

    M(t(1:3,i),t(1:3,i)) = M(t(1:3,i),t(1:3,i)) + Mk;

end
```

B.2 Periodic Boundary Conditions

```
%% Periodic boundary conditions

for i = 1:n_tri

    if  any(i == ind_left_edge)

        ind_opposite = ind_right_edge;

        % Check which two indices in xy_val have
        % the same x value.
```

```
ind_same_xval = logical(sum(repmat(xy_val(1,:),3,1)...
             == repmat(xy_val(1,:)',1,3)) - 1);

% The corresponding indices in the 'p' array.

ind_in_p = t(ind_same_xval,i);

% Compare with saved indices to see check if point has
% already been considered.

if ~isempty(ind_saved)...
 && any(any((ind_in_p...
 == repmat(ind_saved,length(ind_in_p),1))'))

    % Removes an index if it has already been counted.

    ind_in_p = ind_in_p(not(any((ind_in_p...
            == repmat(ind_saved,length(ind_in_p),1)...
                                )')));

end

% Check whether the exclusion of duplicate indices
% empties the variable. If so, skip iteration.

if isempty(ind_in_p)

    continue
```

```
        end

        % Save the indices to not count them multiple times.

        ind_saved(length(ind_saved)+1:...
        length(ind_saved)+length(ind_in_p)) = ind_in_p;

        % Corresponding y values on current edge.

        val_y_cur = p(2,ind_in_p);

        % y values of all points on the opposite side along
        % their indices in p. [y_value index_in_p].

        val_y_op = [p(2,t(1:3,ind_opposite));...
                reshape(t(1:3,ind_opposite),...
               [1 numel(t(1:3,ind_opposite))])]';

        % Comparing y values and finding the indices of the
        % minimum values.

        [~,ind_min_op] = min(abs(val_y_cur - val_y_op(:,1)));

        % The indices in 'p' where these minimum values are
        % located. (The points on the opposite edge which are
        % closest in height to the selected ones on the
        % current edge).

        ind_p_close = val_y_op(ind_min_op,2);
```

```
        k_x = k0 * diel_const.^2 * sin(theta);

        % Inserting boundary conditions.

        M(ind_in_p,:) = 0;

        M(sub2ind(size(M),ind_in_p,ind_in_p)) = 1;

        M(sub2ind(size(M),...
          ind_in_p,ind_p_close)) = -exp(1i*k_x*area_width);

        bv(ind_in_p) = 0;


    end

end
```

B.3 Calculating H'

```
%% Contribution from all cylinder edges.

vec_normal = [];

for i = 1:length(e(1,:))
```

```
if any(ismember(e(6:7,i),obj_zone.scat))

    % Scatterer face on the left or right side of the
    % edge.
    l_or_r = logical(sum(e(6:7,i) == obj_zone.scat,2));

    vec = p(:,e(1:2,i));
    vec_orth = [vec(2,2) - vec(2,1);...
                (vec(1,2) - vec(1,1))]...
            .* (l_or_r - ~l_or_r);
    vec_normal = vec_orth/norm(vec_orth);

    % If current edge is the surface edge inside a
    % scatterer.
    if all(l_or_r)

        H_prime = (vec_normal(1)*cos(theta_2)...
                +  vec_normal(2)*sin(theta_2))...
                *  1i * k0 * n_surf * tran...
                *  exp(1i*k0*n_surf*(cos(theta_2)...
                *  sum(vec(1,:))/2 + sin(theta_2)...
                *  sum(vec(2,:))/2));

        % If the normal vector of the edge points upwards.
        if vec_normal(2) == 1

            u_or_d = logical([1 ; 0]);

        else
```

```
        u_or_d = logical([0 ; 1]);

    end

    switch polarisation

        case 'p'

            di_1 = cyl_diel_const(u_or_d);
            di_ref_1 = env_diel_const(u_or_d);
            di_2 = cyl_diel_const(~u_or_d);
            di_ref_2 = env_diel_const(~u_or_d);

            bk =  (norm(vec_orth)/2)...
               * ((1/di_1 - 1/di_ref_1)...
               -  (1/di_2 - 1/di_ref_2)) * H_prime;

        case 's'

            mag_1 = cyl_mag_const(u_or_d);
            mag_ref_1 = env_mag_const(u_or_d);
            mag_2 = cyl_mag_const(~u_or_d);
            mag_ref_2 = env_mag_const(~u_or_d);

            bk =  (norm(vec_orth)/2)...
               * ((1/mag_1 - 1/mag_ref_1)...
               -  (1/mag_2 - 1/mag_ref_2)) * H_prime;
```

```
        end

    else

        u_or_d = logical(sum(e(6:7,i) == obj_zone.env,2));

        H_prime = [(vec_normal(1)*cos(theta_1)...
                +   vec_normal(2)*sin(theta_1))...
                *   1i * k0 * n_env...
                *   exp(1i*k0*n_env*(cos(theta_1)...
                *   sum(vec(1,:))/2 + sin(theta_1)...
                *   sum(vec(2,:))/2))...
                +   (vec_normal(1)*cos(theta_1)...
                -   vec_normal(2)*sin(theta_1))...
                *   1i * k0 * n_env * refl...
                *   exp(1i*k0*n_env*(cos(theta_1)...
                *   sum(vec(1,:))/2 ...
                -   sin(theta_1)*sum(vec(2,:))/2))...
                ;...
                   (vec_normal(1)*cos(theta_2)...
                +   vec_normal(2)*sin(theta_2))...
                *   1i * k0 * n_surf * tran...
                *   exp(1i*k0*n_surf*(cos(theta_2)...
                *   sum(vec(1,:))/2 ...
                +   sin(theta_2)*sum(vec(2,:))/2))];

        switch polarisation

            case 'p'
```

```
                di_1 = env_diel_const(u_or_d);
                di_ref_1 = env_diel_const(1);
                di_2 = cyl_diel_const(l_or_r);
                di_ref_2 = env_diel_const(2);

                bk =  (norm(vec_orth)/2)...
                   * (((1/di_1 - 1/di_ref_1)...
                   -  (1/di_2 - 1/di_ref_2))...
                   *   H_prime(u_or_d));

            case 's'

                mag_1 = env_mag_const(u_or_d);
                mag_ref_1 = env_mag_const(1);
                mag_2 = cyl_mag_const(l_or_r);
                mag_ref_2 = env_mag_const(2);

                bk =  (norm(vec_orth)/2)...
                   * ((1/mag_1 - 1/mag_ref_1)...
                   -  (1/mag_2 - 1/mag_ref_2))...
                   *   H_prime(u_or_d);

        end

    end

    bv(e(1:2,i)) = bv(e(1:2,i)) + bk;
```

```
    end

end
```

B.4 Elemental Contribution to Total Field

```
%% Contribution from triangles in all scatterers on the total
%  field.

% For all the scatterers in the structure.
for i = 1:length(obj_zone.scat)

    % All the triangles located within the current face.
    tri_in_cyl = t(1:end-1,ismember(t(4,:),obj_zone.scat(i)));

    tri_cyl_x = p(1,tri_in_cyl);
    tri_cyl_y = p(2,tri_in_cyl);
    xy_123_vals = [1:3:length(tri_cyl_x) ;...
                   2:3:length(tri_cyl_x) ;...
                   3:3:length(tri_cyl_x)];

    tri_area = abs((tri_cyl_y(xy_123_vals(3,:))...
              -      tri_cyl_y(xy_123_vals(1,:)))...
             .*     (tri_cyl_x(xy_123_vals(2,:))...
              -      tri_cyl_x(xy_123_vals(1,:)))...
              -     (tri_cyl_y(xy_123_vals(2,:))...
              -      tri_cyl_y(xy_123_vals(1,:)))...
```

```
        .*      (tri_cyl_x(xy_123_vals(3,:))...
         -       tri_cyl_x(xy_123_vals(1,:))))/2;

x_avg = (tri_cyl_x(xy_123_vals(1,:))...
      +  tri_cyl_x(xy_123_vals(2,:))...
      +  tri_cyl_x(xy_123_vals(3,:)))/3;
y_avg = (tri_cyl_y(xy_123_vals(1,:))...
      +  tri_cyl_y(xy_123_vals(2,:))...
      +  tri_cyl_y(xy_123_vals(3,:)))/3;

% If a triangle's mean is above the surface.
if mean(y_avg) > surface_y_coordinate

    di_ref = env_diel_const(1);

    mag_ref = env_mag_const(1);

    H0r =        exp(1i*k0*(sqrt(di_ref))...
        * (cos(theta_1) * x_avg...
        + sin(theta_1) * y_avg))...
        + refl * exp(1i*k0*(sqrt(di_ref))...
        * (cos(theta_1) * x_avg...
        - sin(theta_1) * y_avg));

else

    di_ref = env_diel_const(2);

    mag_ref = env_mag_const(2);
```

```
        H0r = tran .* exp(1i*k0*(sqrt(di_ref))*(cos(theta_2)...
            .* x_avg + sin(theta_2)*y_avg));

    end

    switch polarisation

        case 'p'

            bk = tri_area .* (2/6)...
              .* (di_ref .* (1/cyl_diel_const(i)...
               - 1/di_ref) - (cyl_mag_const(i) - mag_ref))...
              .* k0.^2 .* di_ref .* H0r;

        case 's'

            bk = tri_area .* (2/6)...
              .* (mag_ref .* (1/cyl_mag_const(i)...
               - 1/mag_ref) - (cyl_diel_const(i) - di_ref))...
              .* k0.^2 .* mag_ref .* H0r;

    end

    for j = 1:length(bk)

        % Insert the values in the b vector.
        bv(tri_in_cyl(:,j)) = bv(tri_in_cyl(:,j)) + bk(j);
```

```
    end

end
```